Seasonal Variation of Oxygenated Organic Molecules in Urban Beijing and their Contribution to Secondary Organic Aerosol

Yishuo Guo[1], Chao Yan[1,2,*], Yuliang Liu[3], Xiaohui Qiao[4], Feixue Zheng[1], Ying Zhang[1], Ying Zhou[1], Chang Li[1], Xiaolong Fan[1], Zhuohui Lin[1], Zemin Feng[1], Yusheng Zhang[1], Penggang Zheng[5], Linhui Tian[7], Wei Nie[3], Zhe Wang[5,6], Dandan Huang[8], Kaspar R. Daellenbach[2,9], Lei Yao[1,2], Lubna Dada[2,9], Federico Bianchi[2], Jingkun Jiang[4], Yongchun Liu[1], Veli-Matti Kerminen[2], Markku Kulmala[1,2]

Affiliations:
[1] Aerosol and Haze Laboratory, Beijing Advanced Innovation Center for Soft Matter Science and Engineering, Beijing University of Chemical Technology, Beijing, China

[2] Institute for Atmospheric and Earth System Research / Physics, Faculty of Science, University of Helsinki, Finland

[3] Joint International Research Laboratory of Atmospheric and Earth System Research, School of Atmospheric Sciences, Nanjing University, Nanjing, China

[4] State Key Joint Laboratory of Environment Simulation and Pollution Control, State Environmental Protection Key Laboratory of Sources and Control of Air Pollution Complex, School of Environment, Tsinghua University, Beijing, China

[5] Division of Environment and Sustainability, The Hong Kong University of Science and Technology (HKUST), Hong Kong SAR, China

[6] Department of Civil and Environmental Engineering, The Hong Kong Polytechnic University (HKPolyU), Hong Kong SAR

[7] Department of Civil and Environmental Engineering, Faculty of Science and Technology, University of Macau, Taipa, Macau, China

[8] State Environmental Protection Key Laboratory of Formation and Prevention of Urban Air Pollution Complex, Shanghai Academy of Environmental Sciences, Shanghai, China

[9] Laboratory of Atmospheric Chemistry, Paul Scherrer Institute, Villigen, Switzerland.

Correspondence to: Chao Yan (chao.yan@helsinki.fi)

Abstract Oxygenated organic molecules (OOMs) are crucial for atmospheric new particle formation and secondary organic aerosol (SOA) growth. Therefore, understanding their chemical composition, temporal behavior, and sources is of great importance. Previous studies on OOMs mainly focus on environments where biogenic sources are predominant, yet studies on sites with dominant anthropogenic emissions, such as megacities, have been lacking. Here, we conducted long-term measurements of OOMs covering four seasons of the year 2019 in urban Beijing. The OOM concentration was found to be the highest in summer (1.6×10^8 cm^{-3}), followed by autumn (7.9×10^7 cm^{-3}), spring (5.7×10^7 cm^{-3}) and winter (2.3×10^7 cm^{-3}), suggesting that enhanced photo-oxidation together with the rise of temperature promote the formation of OOMs. Most OOMs contained 5 to 10 carbon atoms and 3 to 7 effective oxygen atoms ($nO_{eff} = nO - 2 \times nN$). The average nO_{eff} increased with increasing atmospheric photo-oxidation capacity, which was the highest in summer and the lowest in winter and autumn. By performing a newly developed workflow, OOMs were classified into four types: aromatic OOMs, aliphatic OOMs, isoprene OOMs, and monoterpene OOMs. Among them, aromatic OOMs (29-41 %) and aliphatic OOMs (26-41 %) were the main contributors in all seasons, indicating that OOMs in Beijing were dominated by anthropogenic sources. The contribution of isoprene OOMs increased significantly in summer (33 %), which is much higher than those in other three seasons (8-10 %).

39   Concentrations of isoprene ($0.2\text{-}5.3\times10^7$ cm^{-3}) and monoterpene ($1.1\text{-}8.4\times10^6$ cm^{-3}) OOMs in Beijing were lower

40   than those reported at other sites, and they possessed lower oxygen and higher nitrogen contents due to high NO_x

41   levels (9.5-38.3 ppbv) in Beijing. With regard to the nitrogen content of the two anthropogenic OOMs, aromatic

42   OOMs were mainly composed of CHO and CHON species, while aliphatic OOMs were dominated by CHON and

43    $CHON_2$ ones. Such prominent differences suggest varying formation pathways between these two OOMs. By

44   combining the measurements and an aerosol dynamic model, we estimated that the SOA growth rate through OOM

45   condensation could reach 0.64 $\mu g \cdot m^{-3} \cdot h^{-1}$, 0.61 $\mu g \cdot m^{-3} \cdot h^{-1}$, 0.41 $\mu g \cdot m^{-3} \cdot h^{-1}$, and 0.30 $\mu g \cdot m^{-3} \cdot h^{-1}$ in autumn, summer,

46   spring, and winter, respectively. Despite the similar concentrations of aromatic and aliphatic OOMs, the former had

47   lower volatilities and, therefore, showed higher contributions (46-62%) to SOA than the latter (14-32%). By contrast,

48   monoterpene OOMs and isoprene OOMs, limited by low abundances or high volatilities, had low contributions of

49   8-12% and 3-5%, respectively. Overall, our results improve the understanding of the concentration, chemical

50   composition, seasonal variation and potential atmospheric impacts of OOMs, which can help formulate refined

51   restriction policy specific to SOA control in urban areas.

52

1. INTRODUCTION

Atmospheric aerosols affect global climate both directly and indirectly (Stocker, 2014) and are known to have a detrimental influence on human health (Lelieveld et al., 2015). Modeling studies have suggested that new particle formation (NPF) dominates the number concentration of particles and is an important contributor to cloud condensation nuclei (CCN) in the global atmosphere (Merikanto et al., 2009;Gordon et al., 2017). In terms of aerosol mass, it has been shown that a significant fraction is composed of secondary organic aerosol (SOA) (Zhang et al., 2007;Jimenez et al., 2009;Hallquist et al., 2009). In both NPF and SOA formation processes, oxygenated organic molecules (OOMs) have been acknowledged as an important contributor, and thus advanced understanding of OOMs is crucial.

The role of OOMs in NPF was first suggested in 2002, but they could not be identified or quantified at that time (O'Dowd et al., 2002). Then, the emergence of atmospheric pressure interface time-of-flight (APi-TOF) mass spectrometer (Junninen et al., 2010;Ehn et al., 2010;Ehn et al., 2012) and Chemical Ionization-APi-TOF (CI-APi-TOF) mass spectrometer (Jokinen et al., 2012;Ehn et al., 2014) provided the first direct measurement of OOMs, which inspired later studies on their role in NPF and SOA growth (Kulmala et al., 2013;Schobesberger et al., 2013;Riccobono et al., 2014;Ehn et al., 2014;Kirkby et al., 2016;Tröstl et al., 2016;Bianchi et al., 2016;Lehtipalo et al., 2018;Rose et al., 2018;Stolzenburg et al., 2018;Mohr et al., 2019;Heinritzi et al., 2020;Yan et al., 2020;Caudillo et al., 2021). These studies found that the functionality and volatility of OOMs are the key factors in determining whether OOM species can participate in NPF (Donahue et al., 2013). More specifically, ultra-low-volatility organic compounds (ULVOCs, whose mass saturation concentrations, C^*, are smaller than 3×10^{-9} µg·m^{-3}, or number saturation concentrations, N^*, are smaller than 6 cm^{-3} by assuming an average molar mass of 300 Da) are the main participator of the initial nucleation at certain conditions (Schervish and Donahue, 2020), and extremely-low-volatility organic compounds (ELVOCs, $3\times10^{-9} < C^* < 3\times10^{-4}$ µg·m^{-3}, $6 < N^* < 6\times10^{5}$ cm^{-3}) and low-volatility organic compounds (LVOCs, $3\times10^{-4} < C^* < 0.3$ µg·m^{-3}, $6\times10^{5} < C^* < 6\times10^{8}$ cm^{-3}) can have a dominant contribution to the growth of newly formed particles.

Owing to the significance of OOMs in atmospheric aerosols formation and growth, its reliable measurement is of high importance. Up till now, the majority of reported sites in the lower troposphere with OOM measurement are non-urban areas, such as forest, agricultural pasture and countryside, where the most abundant OOM species are oxidized products from monoterpenes and isoprene. In the boreal forest of southern Finland, the reported OOM concentration was the highest in summer (4.6×10^{8} cm^{-3}) (Huang et al., 2020), followed by autumn (8.0×10^{7} cm^{-3}) (Zha et al., 2018) and spring (~4.0×10^{7} cm^{-3}) (Yan et al., 2016;Roldin et al., 2019;Bianchi et al., 2017). The level of OOMs also varied significantly at different sites. In Melpitz agricultural-forest of central Europe, OOM concentration (2.5×10^{8} cm^{-3} in summer) (Mutzel et al., 2015) was comparable with that in Hyytiälä, while in Alabama forest of the United States, OOM concentration was much higher (4.8×10^{9} cm^{-3} in summer) (Massoli et al., 2018;Krechmer et al., 2015), possibly due to higher UVB and temperature. Besides, monoterpene OOMs at

Atmospheric
Chemistry
and Physics
Discussions

87   agricultural-rural mixed Vielbrunn were also detected (3.6×10^6 cm^{-3} in spring), and results showed that many other

88   unidentified species also took a large fraction, especially at night (Kürten et al., 2016). All of these studies highlight

89   the importance of OOM measurement worldwide. Several urban observations were also reported (Brean et al.,

90   2019;Ye et al., 2020). Although they showed that OOMs in Chinese urban cities contain a significant fraction of

91   compounds with 6 to 9 carbons and that many contain nitrogen, they either reported concentrations of a few chosen

92   species or just spectral signals. Moreover, due to the limitation of short measurement periods, they were incapable

93   of exploring the seasonal behavior of OOM concentration and detailed composition, which are crucial for fully

94   evaluating their potential contribution to the growth of SOA.

95   In this work, we studied the OOMs measured by a CI-APi-TOF mass spectrometer using nitrate (NO$_3^-$) as reagent

96   ions. The dataset covers four seasons of Year 2019. We performed detailed molecular analyses within the mass to

97   charge ratio between 200-400 Th and identified around 1000 OOMs for each season. The seasonal variations of

98   their concentration, molecular composition, volatility distribution, and potential SOA contribution were

99   systematically investigated for the first time. Furthermore, with a newly developed workflow, we traced their

100   potential sources, including aromatics, aliphatics, monoterpenes, and isoprene. Finally, we evaluated the relative

101   contribution of anthropogenic and biogenic sources in different seasons.

102   **2. MEASUREMENTS AND METHODS**

103   **2.1. Measurements**

104   The measurement was conducted at the west campus of Beijing University of Chemical Technology (39.95° N,

105   116.31° E) on the fifth floor of the teaching building, which is about 15 m above the ground level. This station is a

106   representative urban site, and a detailed description can be found elsewhere (Liu et al., 2020;Yan et al., 2021;Guo

107   et al., 2021).

108   The concentration of OOMs was measured by a nitrate (NO$_3^-$)-CI-APi-TOF mass spectrometer (abbreviated as

109   nitrate CIMS) (Aerodyne Research, Inc.). The basic working principle of this instrument can be found elsewhere

110   (Jokinen et al., 2012), and the detailed sampling configuration is the same as that reported by Yan et al. (Yan et al.,

111   2021). Two steps were included in the quantification of OOM concentration. First, a mass-dependent transmission

112   experiment was conducted according to a previous study (Heinritzi et al., 2016), and the transmission curve was

113   obtained by comparing the decrease of primary ion signals and the increase of added perfluorinated acid signals.

114   Second, the calibration factor of sulfuric acid was applied to estimate OOM concentration. Some studies have shown

115   that OOM molecules with less oxygen number are not ionized as efficiently as sulfuric acid by NO$_3^-$ (Hyttinen et

116   al., 2015;Hyttinen et al., 2018;Riva et al., 2019). Therefore, the reported OOM concentration in this study should

117   be regarded as the lower limit. The concentration of each OOM molecule can be calculated as follows:

118
$$[\text{OOM}] = \frac{\sum_{i=0}^{1} (\text{HNO}_3)_i \text{NO}_3^- (\text{OOM}) + (\text{HNO}_3)_i (\text{OOM} - \text{H})^-}{\sum_{i=0}^{2} (\text{HNO}_3)_i \text{NO}_3^-} \times C \div T_{\text{OOM}}$$

119　The numerator on the right-hand side is the sum of detected signal of that OOM in the unit of counts per second

120　(cps), either as a cluster of a neutral molecule combined with NO_3^-, $(HNO_3)_iNO_3^-(OOM))$, or as a deprotonated ion,

121　$(OOM-H)^-$. It should be pointed out that in nitrate CIMS, most OOMs were detected as the cluster form of NO_3^-

122　(OOM). The denominator is the sum of all reagent ion signals in cps. C is the calibration factor of sulfuric acid,

123　ranging from 6.07×10^9 to 7.47×10^9 cm^{-3} / (normalized cps) during the whole year. Such a narrow range of the

124　calibration factor also indicated that our instrument had a stable performance during the measurement period. T_{OOM}

125　is the relative transmission efficiency of a specific OOM molecule in comparison with that of the reagent ions.

126　　The number concentration of aerosol particles from 6 to 840 nm was measured by a Differential Mobility Particle

127　Sizer (DMPS) (Aalto et al., 2001). The mass concentration of $PM_{2.5}$ was measured with a Tapered Element

128　Oscillating Microbalance Dichotomous Ambient Particulate Monitor (TEOM 1405-DF, Thermo Fisher Scientific

129　Inc, USA). The chemical composition of the $PM_{2.5}$ was obtained from an Aerosol Chemical Speciation Monitor

130　(ACSM) (Jayne et al., 2000;Drewnick et al., 2005), and PMF analysis was further performed to separate secondary

131　organic aerosols from primary ones. Meteorological parameters were measured with a weather station (AWS310,

132　Vaisala Inc.) located on the rooftop of the building. Concentrations of trace gases, including carbon monoxide (CO),

133　sulfur dioxide (SO_2), nitrogen oxides (NO_x), and ozone (O_3), were monitored using Thermo Environmental

134　Instruments (models 48i, 43i-TLE, 42i, 49i, respectively).

135　　The measurement period covers four seasons of the year 2019, including 135 days in total. Winter, spring,

136　summer, and autumn periods range from 5th Jan. to 14th Feb., 15th Mar. to 14th Apr., 10th Jul. to 9th Aug., and 19th

137　Oct. to 18th Nov., respectively.

138　**2.2. A revised workflow for the classification of OOM Sources**

139　　A recently developed workflow, based on the molecular composition as well as the up-to-date knowledge of

140　atmospheric OOM formation chemistry, was used for retrieving their possible sources (Nie et al., 2022) (Xu et al.,

141　2021). In this approach, mass spectral binning combined with positive matrix factorization (binPMF) (Zhang et al.,

142　2019) needs to be performed first to extract the factor of monoterpene OOMs. However, as performing binPMF is

143　time-consuming and not suitable for large data sets as used in this study, we replaced the binPMF step by the criteria

144　of nC=10, $nO_{eff} \geqslant 4$, and $2 \leqslant DBE \leqslant 4$ (Fig. 1) for the selection of monoterpene OOMs. Such standards were set

145　based on their reported composition (Ehn et al., 2012;Yan et al., 2016;Jokinen et al., 2014;Boyd et al., 2015;Berndt

146　et al., 2016;Berndt et al., 2018). Here, nC is the carbon number. nO_{eff} (= nO–2×nN) is the effective oxygen number,

147　which subtracts the number of oxygen bonded to nitrogen by assuming that all nitrogen atoms are in the form of

148　nitrate groups ($-ONO_2$) or peroxynitrate nitrate group ($-OONO_2$). To our best knowledge, this is the common case

149　for all nitrogen-containing compounds formed through the reaction between RO_2 and NO_x (Orlando and Tyndall,

150　2012;Seinfeld and Pandis, 2016). Exceptions are those nitrophenols (Yan et al., 2016;Wang et al., 2019;Song et al.,

151　2021) that were classified separately (Nie et al., 2022). The reason for choosing nO_{eff} rather than nO is that it better

152　reflects the oxidation state of closed-shell molecules as well as their parent RO_2 radicals. For example, $C_7H_9O_5$

153   peroxy radical can produce both $C_7H_{10}O_4$ and $C_7H_9O_6N$ when reacting with NO, and all of them have the same nO_{eff}

154   of four. In addition, nO_{eff} considers the influence of nitrogen and represents volatility more directly (Yan et al.,

155   2020), and thus makes it easier for the volatility comparison among OOMs with different nitrogen atoms.

156   DBE denotes the double bond equivalence and is calculated as $(2nC+2–nH–nN)/2$, which is the same as the term

157   degree of unsaturation. The DBE of one OOM molecule is influenced by both its precursor and the oxidation

158   processes. For example, aromatic VOCs have DBE values no smaller than 4. For their oxidation products, a previous

159   study has shown that under OH exposures equivalent to approximately 10-15 days in typical atmospheric conditions,

160   they possess DBE values no smaller than 2 (Garmash et al., 2020). However, reported monoterpene OOMs also

161   have DBE values the same as those of aromatic OOMs, which makes them difficult to distinguish. According to

162   laboratory studies, the majority of monomer products from monoterpene oxidation are C10 compounds (Yan et al.,

163   2020). Measurement results also showed that the concentrations of C10 aromatic VOCs are very low (Zhang et al.,

164   2017) compared with other C6-C9 ones. Therefore, those C10 OOMs with DBE values of 2 to 4 are likely

165   monoterpene OOMs. For OOMs with DBE values smaller than 2, neither aromatics nor monoterpenes oxidation

166   could explain their formation. Hence, the precursors of those OOMs should be the ones without aromatic rings and

167   have smaller DBE values, such as alkanes, alkenes, and some unsaturated oxygen-containing VOCs (OVOCs).

168   OOMs with DBE values of 2 are rather complex. Their precursors could be aromatics, aliphatics, or other unknown

169   sources, and a detailed discussion of the classification criteria could be found in Nie et al. (Nie et al., 2022). By

170   performing this revised workflow, OOMs were finally divided into five groups: isoprene (IP) OOMs, monoterpene

171   (MT) OOMs, aromatic OOMs, aliphatic OOMs, and a small amount of undistinguished OOMs (6-9 %) that cannot
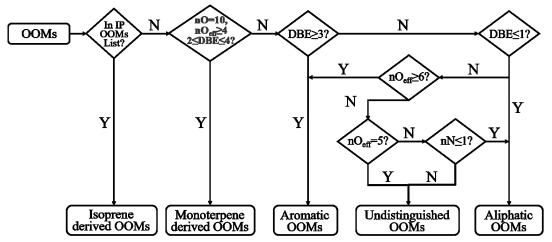
172   be classified into those four types.

173
174   **Figure 1.** Workflow for retrieving OOM sources. "IP OOMs" represents isoprene-derived OOMs. nO_{eff} and nN are the numbers
175   of effective oxygen and nitrogen in each OOM molecule, respectively. "Y" and "N" denote "Yes" and "No", respectively.

Atmospheric
Chemistry
and Physics
Discussions

3. RESULTS AND DISCUSSIONS

3.1. Seasonal Variation of OOM Concentration and Composition

The concentration and molecular composition are the most fundamental characteristics of OOMs. We summarized the OOM concentrations in Beijing and other lower tropospheric sites in Table 1 and Fig. 2 for better comparison. Generally, a clear seasonal trend of OOM concentration in Beijing can be observed, where total OOM concentration is highest in summer (1.6×10^8 cm^{-3}), followed by autumn (7.9×10^7 cm^{-3}) and spring (5.7×10^7 cm^{-3}), and the lowest in winter (2.3×10^7 cm^{-3}). This apparent increase of OOM concentrations with an increased temperature and theoretical global radiation indicates that elevated solar radiation along with higher temperature favors the generation of OOMs. In comparison to other locations, the level of OOMs in urban Beijing varied within the ranges of previously reported ones (Yan et al., 2016;Roldin et al., 2019;Bianchi et al., 2017;Zha et al., 2018;Huang et al., 2020;Mutzel et al., 2015;Massoli et al., 2018;Nie et al., 2022). Interestingly, the above clear correlation between global radiation (or temperature) and OOM concentration can also be seen in other locations, yet OOMs in forest environments are in general higher than in urban or suburban areas. On the one hand, this observation suggests that OOM formation at a specific environment is prevailingly influenced by the strength of atmospheric photochemistry; on the other hand, forest environment appears to have more abundant OOMs than urban environments, possibly because the OOM yield of biogenic VOCs is higher than that of anthropogenic VOCs (Berndt et al., 2016;Teng et al., 2017;Garmash et al., 2020;Molteni et al., 2018). Yet, a quantitative explanation of the OOM variation between seasons and locations requires comprehensive measurements as well as analyses on both the production and loss of OOMs.

Table 1. Mean, standard deviation (Std), median, 25 and 75 percentiles (25th and 75th) of measured OOM concentrations at various lower tropospheric sites.

Measurement Site	Period	Mean (cm^{-3})	Std (cm^{-3})	Median (cm^{-3})	25th (cm^{-3})	75th (cm^{-3})	Reference
Beijing, China	2019 Jan.-Feb.	2.7×10^7	1.7×10^7	2.3×10^7	1.3×10^7	3.6×10^7	This study
Beijing, China	2019 Mar.-Apr.	6.9×10^7	5.1×10^7	5.7×10^7	3.1×10^7	8.9×10^7	This study
Beijing, China	2019 Jul.-Aug.	1.6×10^8	7.5×10^7	1.6×10^8	1.1×10^8	2.2×10^8	This study
Beijing, China	2019 Oct.-Nov.	8.3×10^7	5.2×10^7	7.9×10^7	4.0×10^7	1.2×10^8	This study
Hong Kong, China	2018 Nov.	2.3×10^8	1.1×10^8	2.1×10^8	1.5×10^8	2.9×10^8	2022, Nie et al.
Shanghai, China	2018 Nov.	7.8×10^7	6.3×10^7	6.1×10^7	2.6×10^7	1.2×10^8	2022, Nie et al.
Nanjing, China	2018 Nov.	7.7×10^7	5.4×10^7	7.2×10^7	3.1×10^7	1.1×10^8	2022, Nie et al.
Hyytiälä forest, Finland	2012 Apr.-May	7.5×10^7	6.1×10^7	5.7×10^7	3.6×10^7	9.2×10^7	2016, Yan et al.
Hyytiälä forest, Finland	2013 May	1.4×10^7	7.9×10^6	1.2×10^7	8.1×10^6	1.8×10^7	2019, Roldin et al.
Hyytiälä forest, Finland	2013 Apr.-Jun.	4.5×10^7	1.2×10^7	4.9×10^7	3.2×10^7	5.5×10^7	2017, Bianchi et al.
Hyytiälä forest, Finland	2016 Sep.	1.2×10^8	1.0×10^8	8.0×10^7	3.8×10^7	1.7×10^8	2018, Zha et al.
Melpitz, Germany	2013 Jul.	2.7×10^8	1.7×10^8	2.5×10^8	1.4×10^8	3.5×10^8	2015, Mutzel et al.
Alabama forest, USA	2013 Jun.-Jul.	4.7×10^9	1.5×10^9	4.8×10^9	3.7×10^9	5.3×10^9	2018, Massoli et al.

To further demonstrate the seasonal influence of solar radiation and precursor VOCs on OOMs concentration, we classified OOMs of each season into four groups based on the brightness parameter (Dada et al., 2017) and

201 PM$_{2.5}$ level, respectively. As shown in Fig. S2, in seasons other than summer, OOM concentration under polluted

202 conditions is much higher than that under clean conditions, which likely results from the elevation of precursors

203 coming along with polluted air masses and the accumulation during the pollution. Besides, the concentration of

204 total OOMs on sunny days is higher than that on cloudy days, implying that photochemical oxidation plays a key

205 role in the production of OOM molecules. There is one exception that OOM concentration is not significantly

206 different between sunny and cloudy days under clean condition in autumn, and the cause cannot be concluded in

207 this study without a complete VOC measurement.

208
209 **Figure 2.** OOM concentration vs. temperature at various lower tropospheric sites during daytime (07:00 – 17:00). Data points
210 are colored by theoretical global radiation (GlobRad). Square, circle, and triangle markers represent urban, suburban, and forest
211 areas, respectively. The gray error bars show standard deviations (1σ). Nanjing, Shanghai and Hong Kong datasets are from
212 Nie et al. (Nie et al., 2022), Melpitz data is from Mutzel (Mutzel et al., 2015), Alabama data is from Massoli et al. (Massoli et
213 al., 2018), and Hyytiälä datasets are from Yan et al. (Yan et al., 2016) and Zha et al (Zha et al., 2018).
214
215 For OOM composition, the two-dimensional H/C-O$_{eff}$/C (ratio of hydrogen number to carbon number vs. ratio

216 of effective oxygen number to carbon number) diagrams are plotted to show its characteristics (Fig. S3). And main

217 CHO, CHON, and CHON$_2$ OOM species are also summarized in Table 2. Generally, the composition of OOM

218 molecules exhibits high similarity among different seasons, suggesting no significant changes in OOM formation

219 in general. However, two seasonal characteristics can be found. First, the most oxygenated OOM molecules, such

220 as C$_n$H$_{2n-2}$O$_{6,7}$, C$_n$H$_{2n-4}$O$_{7,8}$ C$_n$H$_{2n+1}$O$_8$N and C$_n$H$_{2n-1}$O$_9$N OOMs, are mainly observed in summer, and meanwhile,

221 the least oxygenated ones, e.g., C$_n$H$_{2n-7}$O$_2$N and C$_n$H$_{2n-9}$O$_{4,5}$N are mostly detected in winter. These observations

222 indicate that, in addition to the enhanced OOM concentration, strong photochemistry also leads to a high oxidation

223 state of OOM. And these summer-specific OOMs can be classified as highly oxygenated organic molecules (HOMs).

224 Second, C$_5$H$_{10}$O$_8$N$_2$ is exceedingly high in summer. A previous study suggested that C$_5$H$_{10}$O$_8$N$_2$ is one dominant

225   oxidation product from isoprene (Xu et al., 2021), and therefore, the high concentration of $C_5H_{10}O_8N_2$ is a clear

226   indication of intensive isoprene oxidation in summer, which will be discussed in detail in Sect. 3.2.

228   **Table 2.** Main CHO, CHON and CHON$_2$ OOM species measured in this study.

DBE	CHO OOMs	CHON OOMs	CHON$_2$ OOMs
0	$C_nH_{2n+2}O_6$	$C_nH_{2n+1}O_{3-8}N$	$C_nH_{2n}O_{4-11}N_2$
1	$C_nH_{2n}O_{2-8}$	$C_nH_{2n-1}O_{3-9}N$	$C_nH_{2n-2}O_{4-10}N_2$
2	$C_nH_{2n-2}O_{3-7}$	$C_nH_{2n-3}O_{3-9}N$	$C_nH_{2n-4}O_{5-11}N_2$
3	$C_nH_{2n-4}O_{2-8}$	$C_nH_{2n-5}O_{3-10}N$	$C_nH_{2n-6}O_{8-11}N_2$
4	$C_nH_{2n-6}O_{3-9}$	$C_nH_{2n-7}O_{3-9}N$	$C_nH_{2n-8}O_{7,8}N_2$
5	$C_nH_{2n-8}O_{3-8}$	$C_nH_{2n-9}O_{4-10}N$	$C_nH_{2n-10}O_{6-10}N_2$

230   For a better understanding of OOM composition variation among seasons, the distributions of nC, nO$_{eff}$, nN, and

231   DBE, as well as their seasonal variations, are further analyzed. It should be pointed out that the concentration

232   $(5.3 \times 10^7$ cm$^{-3})$ and the fraction (33 %) of IP OOMs in summer is much higher than those in other three seasons, and

233   therefore they are plotted in bars with diagonal lines individually (Fig. 3). In terms of carbon content, the majority

234   of OOMs contain 5 to 10 carbon atoms. For OOMs with 6 to 10 carbon atoms, in seasons other than summer, C6

235   are the most abundant, and a decreasing trend can be seen along with an increasing nC, while in summer, an opposite

236   trend is observed, i.e., the relative contribution increases with an increasing nC. The causes behind the different

237   trends in summer and other seasons are complex but might include changes in the precursor VOC distribution,

238   varying reactivity responses of VOCs to temperature, and the volatilities of OOMs that influence their atmospheric

239   lifetime. Further analysis on this topic will be made in the future. For C5 OOMs, the contribution from isoprene

240   varies from less than half in winter and spring to ~70 % in summer. The high contribution of IP OOMs in summer

241   is in line with the strong isoprene emission coupled with the enhanced photo-oxidation (Cheng et al., 2018;Zhang

242   et al., 2020).

243   Concerning the oxygen content, most OOMs contain 3 to 7 effective oxygen atoms, accounting for 86-95 % of

244   total OOMs in all seasons. With the increase of effective oxygen number, the contribution of corresponding OOMs

245   first increases and then decreases, with nO$_{eff}$=4 OOMs having the highest fraction. Fig. S4 shows that the

246   concentration-weighted average nO$_{eff}$ is the highest in summer and lowest in winter and autumn, which is consistent

247   with the observation of individual molecules where the most highly oxygenated ones are usually more abundant in

248   summer. The enhanced multi-step oxidation (Garmash et al., 2020;Wu et al., 2021) and favored auto-oxidation

249   (Molteni et al., 2018;Wang et al., 2017;Wang et al., 2018b;Bianchi et al., 2019) at high temperatures in warmer

250   seasons are most likely the causes. Furthermore, when taking IP OOMs into account, nO$_{eff}$=4 becomes even more

251   prominent in summer, in which $C_5H_{10}O_8N_2$ takes the largest portion and accounts for 77 % of nO$_{eff}$=4 IP OOMs. In

252   winter and autumn, however, nO$_{eff}$=3 has a much higher fraction than those in the other two seasons, and those

253   OOMs are mainly composed of low-DBE compounds, such as $C_nH_{2n}O_7N_2$, $C_nH_{2n-2}O_7N_2$, and $C_nH_{2n-1}O_5N$ species.

254   As for nitrogen content, the vast majority (98-99 %) of OOMs contain 0 to 2 nitrogen atoms, in which CHON

255   OOMs take the largest fraction, varying from 42 % to 51 % among seasons. It should be noted that, although the

256 mixing ratios of NO_x in different seasons change significantly, the nitrogen distributions of non-isoprene OOMs are

257 similar, which is probably due to the fact that NO (0.6-10.0 ppbv) and NO_2 (8.9-28.3 ppbv) concentrations in urban

258 Beijing are always high throughout the year. Those nitrogen atoms could come from either NO_3 radical oxidation

259 or NO_x termination. During the day, nitrogen is likely added mainly through NO_x termination as NO_3 radical should

260 be photolyzed or titrated by NO. However, in the absence of NO_3 photolysis at night, when NO concentration is

261 low, the concentration of NO_3 radical could reach up to ~10 pptv (2.7×10^8 cm^{-3}) in Beijing (Wang et al., 2018a).

262 Under such levels, the NO_3 radial could even dominate the oxidation of biogenic VOCs (i.e., isoprene and

263 monoterpenes) and some aliphatic VOCs, yet oxidation of aromatic VOCs are driven by OH radicals (Table S4

264 and Table S5). Therefore, nitrogen is possibly added through both processes at night.

265   In the case of DBE distribution, most OOMs comprise 0 to 6 DBE values and there is not too much difference

266 among seasons for non-isoprene OOMs. Generally, with the increase of DBE, the fraction of corresponding non-

267 isoprene OOMs first increases and then decreases, with DBE=2 OOMs having the highest contribution (20-29 %).

268 And this is possibly caused by the fact that almost all precursor VOCs, such as aromatics, aliphatics and

269 monoterpenes, can form oxidation products with DBE value of 2. OOMs with DBE larger than 4 and nC no smaller

270 than 10 are likely derived from polycyclic aromatic hydrocarbons (PAHs, DBE≥7), and their fraction varies from

271 5 % in summer to 7-8% in the other three seasons. This demonstrates that PAHs may also have a non-negligible

272 contribution to total OOMs. For IP OOMs, most of them possess 0 or 1 DBE, and only a small fraction (2-16 %) of

273 them retains DBE of precursor isoprene. This means that isoprene oxidation mostly causes a DBE reduction, such

274 as via OH addition to the double carbon bond and the formation of hydroxyl or hydroperoxyl groups; on the contrary,

275 DBE-augment processes, such as the formation of carbonyl and epoxide, are not facilitated. Specifically, in summer,

276 when $C_5H_{10}O_8N_2$ is exceptionally high, the fraction of DBE=0 IP OOMs reaches 75 %, suggesting that few double

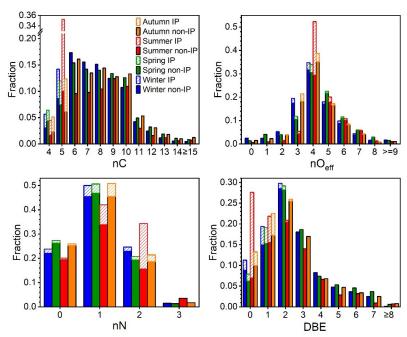277 bond is retained and that the formation of carbonyl or epoxide groups is of less importance in the isoprene oxidation.

Figure 3. Number of carbon (nC), effective oxygen (nO_{eff}), nitrogen (nN), and double bond equivalence (DBE) distribution of OOMs for four seasons. The abbreviations "IP" and "non-IP" represent IP OOMs and other non-isoprene OOMs, respectively. The bars with diagonal lines and filled colors represent IP OOMs and non-isoprene OOMs, respectively.

3.2. Characteristics of Source-classified OOMs

With the workflow described in Sec.2.2, total OOMs were classified into four types: IP OOMs, MT OOMs, aromatic OOMs, and aliphatic OOMs. As shown in Fig. 4, the seasonal concentrations of OOMs from different sources vary with the same trend, highest in summer, followed by autumn, spring, and winter. During the whole year, aromatic OOMs (29-41 %) and aliphatic OOMs (26-41 %) are the most abundant categories, demonstrating that OOMs in Beijing are dominantly from anthropogenic sources. This is also consistent with the observation of SOA composition in previous studies (Le Breton et al., 2018;Mehra et al., 2021). In terms of OOMs from biogenic sources, IP OOMs show a prominent contribution in summer (33 %), which is much higher than those in other seasons (8-10 %). Although it is recently suggested that isoprene can have both biogenic and anthropogenic sources (Wagner and Kuttler, 2014;Panopoulou et al., 2020), the much higher enhancement of IP OOMs in summer can only be explained by the large additional biogenic emission (Cheng et al., 2018;Mo et al., 2018). For MT OOMs, however, the fractional contribution does not show a seasonal variation as clear as that of IP OOMs – it only varies between 5 % and 6 %.
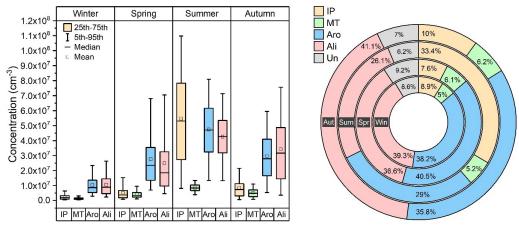
Figure 4. Concentration (left panel) and fraction (right panel) of source-classified OOMs in four seasons. The abbreviations "IP" "MT" "Aro" "Ali" and "Un" stand for IP OOMs, MT OOMs, aromatic OOMs, aliphatic OOMs and undistinguished OOMs respectively. "Win" "Spr" "Sum" and "Aut" represent winter, spring, summer and autumn separately.

3.2.1 Characteristics of biogenic OOMs

The spectral profiles and the fractions of IP OOMs with different nitrogen numbers in four seasons are shown in Fig. 5. Prominent IP OOM species include $C_4H_6O_4$, $C_5H_8O_4$, $C_4H_7O_{6,7}N$, $C_5H_9O_{5-7}N$, $C_5H_{10}O_{7,8}N_2$ and $C_5H_9O_{10}N_3$. CHON$_3$ OOM ($C_5H_9O_{10}N_3$) is detected in all four seasons, suggesting that multi-generation oxidation is involved throughout the year. Besides, the composition of IP OOMs exhibits clear seasonal variation. First, compared with other three seasons, $C_5H_{10}O_8N_2$ and $C_5H_9O_{10}N_3$ have much higher contributions in summer, indicating that NO$_x$ may be involved more efficiently in the oxidation process of isoprene despite its lower concentration (Fig. S6 and Table S1). In addition, nighttime NO$_3$ radicals produced efficiently during summer nights (Wang et al., 2018a) should also promote their formation. Second, despite the overall lowest concentrations of IP OOMs in winter, $C_4H_8O_7$ exhibits a maximum concentration (Fig. S5) and the highest fraction, implying that it may has additional sources other than isoprene oxidation in winter. Third, due to the influence of $C_5H_{10}O_8N_2$ and $C_5H_9O_{10}N_3$, CHON$_2$ and CHON$_3$ IP OOMs take extremely large proportion (~ 67 %) in summer. And interestingly, the seasonal trend of nitrate IP OOM fraction (from largest to smallest is summer, autumn, spring and winter) did not follow the variation of NO$_x$ concentration (from highest to lowest is autumn, winter, spring and summer, Fig. S1 and Table S1), which suggests that the formation of nitrate IP OOMs probably has a non-linear response to NO$_x$.

The concentrations of these prominent IP OOM molecules during summertime in Beijing, Nanjing (32.12° N, 118.95° E) (Liu et al., 2021) and Alabama mixed-forest (32.90° N, 87.25° W) (Krechmer et al., 2015;Massoli et al., 2018) are further compared (Fig. 6). Please note that these molecules plotted are not all the IP OOMs but rather selected abundant ones reported in the literature and in this study. As shown in Fig. 6 (A), IP OOMs exhibit the highest concentration in Alabama forest and the lowest one in Beijing, and the level of IP OOMs in Beijing and Nanjing are comparable. This concentration difference is likely caused by the variation of biogenic isoprene

321 emissions, since Alabama measurement was conducted in a forest, Nanjing site is a suburban area with large

322 vegetation coverage nearby, and Beijing site is located in urban downtown. Besides, the overall varying patterns of

323 IP OOM species in Beijing and Nanjing are very similar, indicating that isoprene in those two urban sites undergo

324 similar oxidation pathways. In terms of oxygen distribution, Beijing and Nanjing are rather similar in that $nO_{eff}=4$

325 OOMs contribute the most, whereas in Alabama $nO_{eff}=5$ ones are the most abundant (Fig. 6 (B)). This lower oxygen

326 content in urban cities is probably caused by the high NO_x levels (11.1 ppbv, 8.5 ppbv and 0.5 ppbv for Beijing,

327 Nanjing and Alabama respectively, Fig. S6), since NO_x efficiently suppresses the oxygen addition of RO_2 radicals

328 (Zhao et al., 2018). Furthermore, the different NO_x levels among the three sites also influence the nitrogen content

329 that Beijing is the highest and Alabama is the lowest (Fig. 6 (C)).

330   From the perspective of diurnal variation, CHO IP OOMs in Beijing possess one daytime peak, while CHON

331 OOMs mainly contain day-night-dual-peak or nocturnal-peak-only types (Fig. S7), which is similar to that reported

332 in Alabama forest (Massoli et al., 2018). But it should be noted that the diurnal variations of some CHON IP OOMs

333 with same molecular composition in this study and Massoli et al. (2018) are not identical, suggesting that their

334 formation pathways are different under various atmospheric conditions.
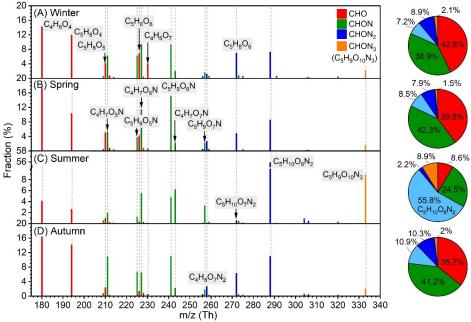

335
336 **Figure 5.** Fractional profiles of each IP OOM molecule in (A) winter, (B) spring, (C) summer and (D) autumn. The mass to
337 charge ratio (m/z) denotes OOM clustered with NO_3^- or as deprotonated ones. The red, green, blue and orange bars are for
338 CHO, CHON, CHON$_2$ and CHON$_3$ OOMs respectively. Please note that CHON$_3$ OOMs only include $C_5H_9O_{10}N_3$.
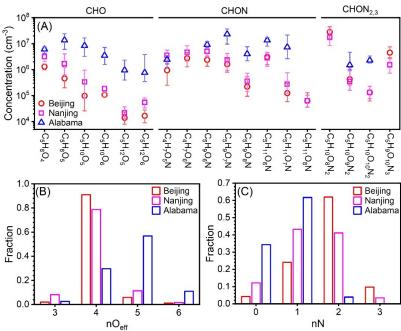
Figure 6. (A) Concentration comparison of specific fingerprint IP OOM molecules between our study and previously reported ones (Krechmer et al., 2015;Massoli et al., 2018;Liu et al., 2021). The markers are median concentration values, and the upper and lower range of the error bar denote 25th and 75th percentiles respectively. Distribution of (B) effective oxygen number, nO_{eff}, and (C) nitrogen number, nN, of IP OOMs plotted in figure (A).

Different from IP OOMs, the overall composition distributions of MT OOMs in the four seasons are quite similar and vary with identical oxygen addition patterns (Fig. 7). Predominant MT OOM molecules are $C_{10}H_{14}O_{4-8}$, $C_{10}H_{16}O_{4-6}$, $C_{10}H_{18}O_{4,5}$, $C_{10}H_{13,15,17}O_{6-9}N$ and $C_{10}H_{14,16}O_{8-10}N_2$. Besides, most MT OOMs belong to CHON category (54-59 %), and the CHO (18-21 %) and $CHON_2$ (19-27 %) ones, with a comparable contribution during the year.

Then, for a better understanding of MT OOM characteristics under different atmospheric environments, representative MT OOM molecules in summer Beijing, spring Hyytiälä forest (61.8° N) (Yan et al., 2016) and summer Alabama mixed-forest (Massoli et al., 2018) are further compared. The following differences can be identified. First, MT OOM concentrations are the highest in Alabama and the lowest in urban Beijing (Fig. 8 (A)), which should result from the synergetic influence of UVB, temperature and precursor monoterpenes. Second, the levels of the two MT radicals that have high concentrations in the Hyytiälä forest, $C_{10}H_{15}O_8\cdot$ and $C_{10}H_{15}O_{10}\cdot$, are not detected in Beijing. This is possibly caused by both low monoterpene abundance (Cheng et al., 2018) and high NO_x concentration in Beijing (11.06 ppbv, Fig. S6), which lead to a low production rate and high loss rate of RO_2 radicals. Third, most MT OOMs in urban Beijing possess 5 or 6 effective oxygen, whereas in the forest environment a large fraction of them can hold 7 to 10 effective oxygen (Fig. 8 (B)). This again suggests that high NO_x in Beijing effectively inhibits the oxygen addition processes (Zhao et al., 2018;Orlando and Tyndall, 2012). Additionally, high NO_x in Beijing also leads to high nitrogen content (Fig. 8 (C)) by promoting the termination reaction between RO_2

Atmospheric
Chemistry
and Physics
Discussions
Open Access
EGU

361   and NO_x (Orlando and Tyndall, 2012) and facilitating the formation of NO_3 radical (Wang et al., 2018a), which

362   further leads to the formation of nitrate MT OOMs (Boyd et al., 2015;Nah et al., 2015).
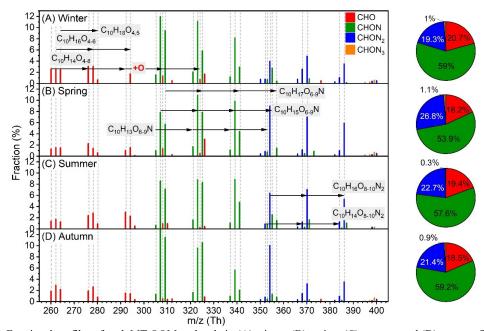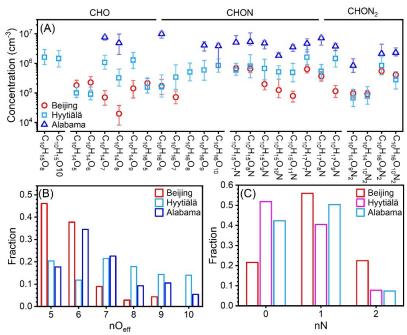

363
364   **Figure 7.** Fractional profiles of each MT OOM molecule in (A) winter, (B) spring, (C) summer and (D) autumn. The mass to
365   charge ratio (m/z) denotes OOM clustered with NO_3^- or as deprotonated ones. The red, green, blue and orange bars are for
366   CHO, CHON, $CHON_2$ and $CHON_3$ OOMs respectively.
367

Figure 8. (A) Concentration comparison of specific fingerprint MT OOM molecules between our study and previously reported ones (Massoli et al., 2018; Yan et al., 2016). The markers are median concentration values, and the upper and lower range of the error bar denote 25th and 75th percentiles respectively. Please note that only the summer Beijing data was plotted as the overall pattern of MT OOMs in Beijing summer and spring are very similar (Fig. 7). Distribution of (B) effective oxygen number, nO_{eff}, and (C) nitrogen number, nN, of MT OOMs plotted in figure (A).

3.2.2 Characteristics of anthropogenic OOMs

Although the oxidation pathways and product composition of a few aromatic VOCs have been studied previously, the reported products are of much less diversity compared to the complex real atmosphere. Therefore, we rely on the workflow (see Sect. 2.2 and Nie et al. 2022) to find out possible aromatic OOMs in our measurement. Among the deduced aromatic OOMs, almost all C6-C9 CHO and C6 CHON compounds have been detected in previous benzene, toluene, xylene, ethylbenzene and mesitylene experiments (Molteni et al., 2018; Garmash et al., 2020) (see detail in Table S8), which demonstrates the reliability of our workflow.

As shown in Fig. 9 (A) to (D), predominant aromatic species in different seasons possess high similarity and they could be classified into $C_{6-9}H_{8-14}O_4$, $C_{6-8}H_{8-12}O_5$, $C_{7,8}H_{8,10}O_5$, $C_{6-10}H_{7-15}O_6N$, $C_{7-9}H_{9-13}O_7N$, $C_{8-10}H_{11-15}O_8N$ and $C_{8,9}H_{12-14}O_{10}N_2$ categories, among which a prominent CH_2 spacing is seen. Such patterns are most likely due to the co-existence of homologous precursor VOCs, although fragmentation processes during the oxidation could also play a role (Pan and Wang, 2014; Zaytsev et al., 2019; Xu et al., 2020). Besides, the distribution of CHON aromatic OOMs in winter and autumn are very similar, with $C_8H_{11}O_6N$ being the highest; in comparison, the overall distribution moves to higher oxygen content in summer, e.g., $C_8H_{11}O_7N$ becomes the largest one. This suggests that enhancement of radiation, which leads to strong photochemistry and high temperature, and the reduction of NO_x in

Atmospheric
Chemistry
and Physics
Discussions

390 summer benefit the formation of highly oxygenated organic molecules (Garmash et al., 2020;Orlando and Tyndall,

391 2012). There are also fingerprint molecules for different seasons, such as $C_{10}H_8O_6$ in spring, $C_9H_{10}O_{11}N_2$ in summer,

392 and $C_{10}H_6O_4$ in summer and autumn. Due to the complexity of real atmosphere, the reason for their seasonal

393 variation is unclear, and further analysis is warranted. In terms of nitrogen content, aromatic OOMs contain large

394 fraction of CHO (42-52 %) and CHON (39-51 %) species. The contribution of $CHON_2$ OOMs reaches the highest

395 in summer, which again indicates that the involvement of NO_x is enhanced under the influence of elevated UVB

396 and temperature. The carbon distribution among seasons are very similar (Fig. S9), where C4 to C9 aromatic OOMs,

397 probably derived from monocyclic aromatic hydrocarbons, make up 68-76 %, and other C≥10 ones, of which 59-

398 68 % are likely the oxidation products from PAHs (DBE≥5) (Table S9), take up 24-32 %. This implies that the

399 relative abundance of emitted aromatic precursors with different carbon atoms is quite stable during the year.

400　　Major aliphatic OOM molecules in different seasons are highly similar, and they possess more evident

401 homologous patterns than aromatic OOMs (Fig. 9 (E) to (H) and Table S10). The dominant species of aliphatic

402 OOMs are $C_{6-9}H_{10-16}O_4$, $C_{6-10}H_{11-19}O_6N$, $C_{5-10}H_{7-17}O_6N$, $C_{5-10}H_{8-18}O_8N_2$ and $C_{6-9}H_{12-18}O_7N_2$, and some less oxygenated

403 compounds, e.g., $C_{6-8}H_{11-15}O_5N$, also have considerable contributions in winter and autumn. For nitrogen content,

404 CHO aliphatic OOMs take smaller fractions in all seasons (8-11 %) in comparison to aromatic CHO OOMs (42-

405 52 %). This implies that NO_x termination may dominate the formation of aliphatic close-shell molecules, or that the

406 branching ratio of the aliphatic RO_2 - NO_x reaction is higher than that of the aromatic one. Besides, unlike aromatic

407 OOMs, aliphatic $CHON_2$ OOMs have a bigger contribution in winter than in the other three seasons. This is because

408 a major sequence of $CHON_2$ OOMs, $C_{6-14}H_{12-28}O_7N_2$, is found to be coincided with $PM_{2.5}$ (Fig. S10), which is

409 frequently high in winter. $C_{6-14}H_{12-28}O_7N_2$ OOMs are classified as either SVOCs or IVOCs (Table S11). Therefore,

410 such a good correlation indicates that $C_{6-14}H_{12-28}O_7N_2$ OOMs themselves, or their precursor VOCs, are able to

411 transport long distance along with $PM_{2.5}$. It is very likely that they are equilibrated in larger gas-phase concentrations

412 as SOA also increases with the elevation of $PM_{2.5}$ (Fig. S11). Those pollution-related OOMs take the largest (14 %)

413 and smallest (2 %) fraction in winter and summer respectively (Table S9). In terms of carbon distribution, there is

414 not too much difference among seasons, in which the relatively short C4 to C9 aliphatic OOMs make up 83-90 %

415 and the longer ones take up 10-17 % (Fig. S9).

Atmospheric
Chemistry
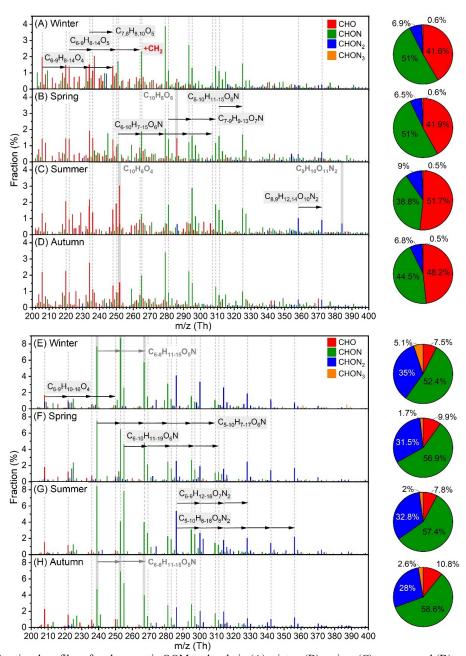and Physics
Discussions

Open Access
EGU

Figure 9. Fractional profiles of each aromatic OOM molecule in (A) winter, (B) spring, (C) summer and (D) autumn, and of each aliphatic OOM molecule in (E) winter, (F) spring, (G) summer and (H) autumn. The mass to charge ratio (m/z) denotes OOM clustered with NO_3^- or as deprotonated ones. The red, green, blue and orange bars are for CHO, CHON, $CHON_2$ and $CHON_3$ OOMs respectively. Species marked with grey dashed lines are primary ones during the year, and species in grey background are special ones for specific seasons.

424   Up till now, field measurements of anthropogenic OOMs are rare (Liu et al., 2021;Nie et al., 2022). In general,

425   the concentrations of aromatic and aliphatic OOMs in Beijing are comparable with those in other Chinese

426   megacities (Table S12), and fingerprint aromatic and aliphatic OOM molecules in Beijing and Nanjing are also

427   identical (Table S13). This suggests that the OOM production, including both the precursor emissions and oxidation

428   mechanisms, may share high similarities in megacities. Yet, a more systematic comparison can only be made when

429   measurements at more locations are available in the future.

430

431   **3.3. Atmospheric implication: OOM contribution to SOA through condensation**

432   The volatility of organic compound determines its partitioning between gas and particle phases, and thus

433   influences its atmospheric lifetime, gas-phase concentration, and contribution to SOA. Therefore, we analyze the

434   characteristics of OOM volatility and summarize the results in Fig. 10. The seasonal variations of OOMs classified

435   as ELVOCs (extremely low-volatility organic compounds), LVOCs (low-volatility organic compounds) and

436   SVOCs (semi-volatile organic compounds) follow the same trend as that of total OOMs, with the highest

437   concentrations in summer (1.3×10^7 cm^{-3}, 4.0×10^7 cm^{-3} and 8.4×10^7 cm^{-3} for ELVOCs, LVOCs, and SVOCs,

438   respectively) and the lowest ones in winter (4.4×10^6 cm^{-3}, 9.4×10^6 cm^{-3} and 5.3×10^6 cm^{-3} for ELVOCs, LVOCs, and

439   SVOCs, respectively). Here, we focus particularly on OOMs with relatively low volatility with high potential

440   contributing to the formation of SOA.

441   Due to the concentration variation of four source-classified OOMs and their temperature-dependent volatility

442   distribution (Table S15), their fractions within different volatility ranges have distinct seasonal characteristics (Fig.

443   10 (B)). Among ELVOCs, aromatic OOMs take the largest fractions, ranging from 72 to94 % throughout the year.

444   For LVOCs, aromatic (34-51 %) and aliphatic OOMs (17-42 %) are the two that have the largest proportions. And

445   MT OOMs, favored by its low volatility (Table S15) (Tröstl et al., 2016;Yan et al., 2020), also take up 14 % of

446   LVOCs in seasons other than winter. IP OOMs, however, due to its high volatility (Table S15) (Krechmer et al.,

447   2015;Xu et al., 2021), do not have an appreciable contribution to ELVOCs and LVOCs even in summer when its

448   concentration is exceedingly high. Consequently, it is likely that the pure condensation of IP OOMs has little

449   contribution to SOA growth regardless of the season.
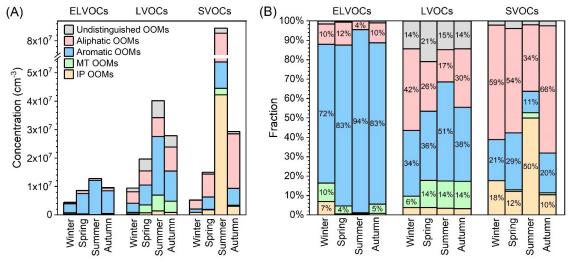
Figure 10. (A) Concentration and (B) fraction of source-classified OOMs in ELVOCs (extremely low volatile organic compounds), LVOCs (low volatile organic compounds) and SVOCs (semi-volatile organic compounds) in four seasons. Please also note that the fractions smaller than 4% are not marked.

The rate of OOM condensation onto particles, referred to as condensation flux hereafter, was calculated based on the particle dynamic model proposed by Trostl et al. (Tröstl et al., 2016) (see details in Sec. S2). In terms of seasonal variation (Fig. 11 (A)), OOM condensation flux exhibits the highest level in autumn (0.64 $\mu g \cdot m^{-3} \cdot h^{-1}$), followed by summer (0.61 $\mu g \cdot m^{-3} \cdot h^{-1}$), spring (0.41 $\mu g \cdot m^{-3} \cdot h^{-1}$), and decreases to the lowest in winter (0.30 $\mu g \cdot m^{-3} \cdot h^{-1}$). For seasonal comparison of SOA formation rate caused by OOM condensation, the characteristic accumulation time (AccTime), defined as SOA divided by OOM condensation flux, is calculated as an indicator (see details in Sec. S3). As shown in Fig. 11 (B), a characteristic time of 24 hours is enough to explain the observed SOA concentration by OOM condensation in winter, and it is reduced to 7 hours, 10 hours, and 7 hours for spring, summer, and autumn, respectively. It should be noted that this should not be interpreted as the entire SOA being formed via OOM condensation during this characteristic time, but rather that OOM condensation is efficient and can have a significant contribution to SOA formation. A recent study (Nie et al., 2022) suggested that OOM condensation can account for about 40% of the SOA formation in wintertime Beijing. Our analysis on seasonal variation indicates that the condensation of OOMs could have a larger contribution to SOA formation in seasons other than winter.

For OOMs from different sources, aromatic OOMs contributes the most during the year, varying from 46 % to 62 %, followed by aliphatic OOMs (14-32 %). In comparison, the two biogenic ones, MT OOMs (8-12 %) and IP OOMs (3-5 %), have smaller contribution in all the four seasons. This indicates that the formation of SOA through condensation in urban Beijing is dominated by anthropogenic sources, which is in line with the previously reported SOA composition (Le Breton et al., 2018;Mehra et al., 2021). Overall, our results suggest that in order to control the formation of SOA, the emission of anthropogenic VOCs, especially aromatics, should be restricted with a high priority.
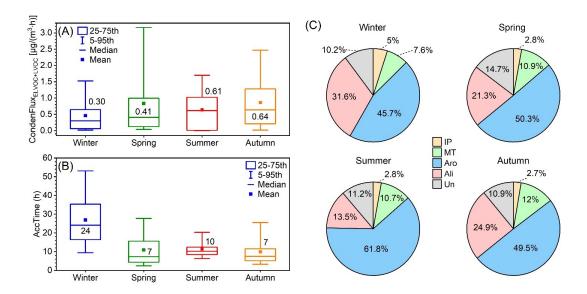
Figure 11. (A) Condensation flux of OOMs calculated by the particle dynamic model by Trostl et al. (Tröstl et al., 2016) in four seasons**.** (B) Characteristic accumulation time of SOA (AccTime), calculated as SOA divided by OOM condensation flux, in four season. This parameter is used as indicator for the relative accumulation rate of SOA caused by OOM condensation in different seasons. The values in each box of (A) and (B) are the median values of corresponding parameters. (C) Estimated condensation flux contribution of four source-classified OOMs in four seasons. The abbreviations "IP" "MT" "Aro" "Ali" and "Un" stand for IP OOMs, MT OOMs, aromatic OOMs, aliphatic OOMs and undistinguished OOMs respectively.

4. Summary and Conclusions

A long-term measurement of OOMs was conducted in urban Beijing. Total OOM concentration in Beijing shows a clear dependence on UVB and temperature, suggesting the importance of photo-oxidation and temperature on OOM formation. In comparison to other atmospheric sites, total OOM concentration in Beijing (2.3×10^7 - 1.6×10^8 cm^{-3}) is generally comparable to urban and suburban areas, and is clearly lower than those measured in forested areas. In the case of composition, most OOMs have 5 to 10 carbon atoms, 3 to 7 effective oxygen atoms, 0 to 2 nitrogen atoms and 0 to 6 DBE values. The seasonal variation of average effective oxygen atom follows the same trend as the overall atmospheric oxidation capacity, being the highest in summer and the lowest in winter and autumn. While for nitrogen and DBE distribution, there are not too much difference among seasons disregarding isoprene OOMs, indicating that the dominant formation pathways of OOMs stay the same during the year.

With a revised workflow, we further separate OOMs into isoprene, monoterpene, aromatic, and aliphatic OOMs. For relative abundance, aromatic (29-41 %) and aliphatic OOMs (26-41 %) are major contributors throughout the year, suggesting that OOMs in urban atmospheric environment are controlled by anthropogenic activities. In addition, isoprene OOMs play an important role in summer and their fraction reaches to 33 %, indicating that biogenic sources are also large contributors to total OOMs in warmer seasons. The concentration of isoprene OOMs

499 (0.2-5.3×10^7 cm^{-3}) and monoterpene OOMs (1.1-8.4×10^6 cm^{-3}) are smaller than those in forest areas, and they

500 exhibit higher nitrogen and lower oxygen content compared with other cleaner sites. One recent study (Nie et al.,

501 2022) reported that the composition of wintertime OOMs among four Chinese megacities, including Beijing, were

502 similar. Our study further demonstrates that the composition of summertime OOMs between Beijing and Nanjing

503 also have strong resemblance. Consequently, the seasonal characteristics of Beijing OOMs in this study could be

504 representative of OOMs in other Chinese metropolises.

505 In terms of volatility, monoterpene OOMs are the most condensable, isoprene OOMs are the most volatile, and

506 aromatic OOMs are more condensable than aliphatic ones. Based on the volatility and concentration characteristics

507 of the four source-classified OOMs, an aerosol growth model was utilized to calculate their contribution to SOA

508 growth. Results show that the condensation flux of total OOMs (0.30-0.64 μg·m^{-3}·h^{-1}) are high enough to produce

509 a considerable amount of SOA within a day, and that aromatic (46-62 %) and aliphatic (14-32 %) OOMs are found

510 to be dominant contributors regardless of seasons. This suggests that the formation of SOA in urban cities are likely

511 driven by OOMs from anthropogenic sources, and highlights the importance of reducing anthropogenic emissions,

512 especially aromatics, for pollution mitigation.

513

514 **Data and materials availability:** Data and materials are available upon contacting the first author and
515 corresponding author.
516

517 **Author contributions:** CY and YG designed the study and wrote the manuscript. YG, YL, FZ, Ying Zhang, Ying
518 Zhou, CL, XF, ZL, ZF, Yusheng Zhang, PZ and LT conducted the measurement and collected the data. CY, WN,
519 ZW, DH, XQ, YL, YG, PZ and LT built the workflow and contributed to the aerosol dynamic model. JJ and VMK
520 modified the manuscript. And all co-authors have read and commented on the manuscript.

521

522 **Competing interests:** The authors declare no competing interest.

523

526 **References**

527 Aalto, P., Hämeri, K., Becker, E., Weber, R., Salm, J., Mäkelä, J. M., Hoell, C., O'dowd, C. D., Hansson, H.-C.,
528 Väkevä, M., Koponen, I. K., Buzorius, G., and Kulmala, M.: Physical characterization of aerosol particles during
529 nucleation events, Tellus B: Chemical and Physical Meteorology, 53, 344-358, 10.3402/tellusb.v53i4.17127, 2001.

530

531 Berndt, T., Richters, S., Jokinen, T., Hyttinen, N., Kurtén, T., Otkjær, R. V., Kjaergaard, H. G., Stratmann, F.,
532 Herrmann, H., Sipilä, M., Kulmala, M., and Ehn, M.: Hydroxyl radical-induced formation of highly oxidized
533 organic compounds, Nature Communications, 7, 13677, 10.1038/ncomms13677, 2016.

534

535   Berndt, T., Mentler, B., Scholz, W., Fischer, L., Herrmann, H., Kulmala, M., and Hansel, A.: Accretion Product
536   Formation from Ozonolysis and OH Radical Reaction of α-Pinene: Mechanistic Insight and the Influence of
537   Isoprene and Ethylene, Environmental Science & Technology, 52, 10.1021/acs.est.8b02210, 2018.
538
539   Bianchi, F., Tröstl, J., Junninen, H., Frege, C., Henne, S., Hoyle, C. R., Molteni, U., Herrmann, E., Adamov, A.,
540   Bukowiecki, N., Chen, X., Duplissy, J., Gysel, M., Hutterli, M., Kangasluoma, J., Kontkanen, J., Kürten, A.,
541   Manninen, H. E., Münch, S., Peräkylä, O., Petäjä, T., Rondo, L., Williamson, C., Weingartner, E., Curtius, J.,
542   Worsnop, D. R., Kulmala, M., Dommen, J., and Baltensperger, U.: New particle formation in the free troposphere:
543   A question of chemistry and timing, Science, 352, 1109-1112, 10.1126/science.aad5456, 2016.
544
545   Bianchi, F., Garmash, O., He, X., Yan, C., Iyer, S., Rosendahl, I., Xu, Z., Rissanen, M. P., Riva, M., Taipale, R.,
546   Sarnela, N., Petäjä, T., Worsnop, D. R., Kulmala, M., Ehn, M., and Junninen, H.: The role of highly oxygenated
547   molecules (HOMs) in determining the composition of ambient ions in the boreal forest, Atmos. Chem. Phys., 17,
548   13819-13831, 10.5194/acp-17-13819-2017, 2017.
549
550   Bianchi, F., Kurten, T., Riva, M., Mohr, C., Rissanen, M. P., Roldin, P., Berndt, T., Crounse, J. D., Wennberg, P.
551   O., Mentel, T. F., Wildt, J., Junninen, H., Jokinen, T., Kulmala, M., Worsnop, D. R., Thornton, J. A., Donahue, N.,
552   Kjaergaard, H. G., and Ehn, M.: Highly Oxygenated Organic Molecules (HOM) from Gas-Phase Autoxidation
553   Involving Peroxy Radicals: A Key Contributor to Atmospheric Aerosol, Chemical Reviews, 119, 3472-3509,
554   10.1021/acs.chemrev.8b00395, 2019.
555
556   Boyd, C. M., Sanchez, J., Xu, L., Eugene, A. J., Nah, T., Tuet, W. Y., Guzman, M. I., and Ng, N. L.: Secondary
557   organic aerosol formation from the β-pinene+NO$_3$ system: effect of humidity and peroxy radical fate,
558   Atmos. Chem. Phys., 15, 7497-7522, 10.5194/acp-15-7497-2015, 2015.
559
560   Brean, J., Harrison, R. M., Shi, Z., Beddows, D. C. S., Acton, W. J. F., Hewitt, C. N., Squires, F. A., and Lee, J.:
561   Observations of highly oxidized molecules and particle nucleation in the atmosphere of Beijing, Atmos. Chem.
562   Phys., 19, 14933-14947, 10.5194/acp-19-14933-2019, 2019.
563
564   Caudillo, L., Rörup, B., Heinritzi, M., Marie, G., Simon, M., Wagner, A. C., Müller, T., Granzin, M., Amorim, A.,
565   Ataei, F., Baalbaki, R., Bertozzi, B., Brasseur, Z., Chiu, R., Chu, B., Dada, L., Duplissy, J., Finkenzeller, H.,
566   Gonzalez Carracedo, L., He, X. C., Hofbauer, V., Kong, W., Lamkaddam, H., Lee, C. P., Lopez, B., Mahfouz, N.
567   G. A., Makhmutov, V., Manninen, H. E., Marten, R., Massabò, D., Mauldin, R. L., Mentler, B., Molteni, U., Onnela,
568   A., Pfeifer, J., Philippov, M., Piedehierro, A. A., Schervish, M., Scholz, W., Schulze, B., Shen, J., Stolzenburg, D.,
569   Stozhkov, Y., Surdu, M., Tauber, C., Tham, Y. J., Tian, P., Tomé, A., Vogt, S., Wang, M., Wang, D. S., Weber, S.
570   K., Welti, A., Yonghong, W., Yusheng, W., Zauner-Wieczorek, M., Baltensperger, U., El Haddad, I., Flagan, R. C.,
571   Hansel, A., Höhler, K., Kirkby, J., Kulmala, M., Lehtipalo, K., Möhler, O., Saathoff, H., Volkamer, R., Winkler, P.
572   M., Donahue, N. M., Kürten, A., and Curtius, J.: Chemical composition of nanoparticles from α-pinene nucleation
573   and the influence of isoprene and relative humidity at low temperature, Atmos. Chem. Phys. Discuss., 2021, 1-26,
574   10.5194/acp-2021-512, 2021.
575

576 Cheng, X., Li, H., Zhang, Y., Li, Y., Zhang, W., Wang, X., Bi, F., Zhang, H., Gao, J., Chai, F., Lun, X., Chen, Y.,
577 Gao, J., and Lv, J.: Atmospheric isoprene and monoterpenes in a typical urban area of Beijing: Pollution
578 characterization, chemical reactivity and source identification, Journal of Environmental Sciences, 71, 150-167,
579 https://doi.org/10.1016/j.jes.2017.12.017, 2018.
580
581 Dada, L., Paasonen, P., Nieminen, T., Buenrostro Mazon, S., Kontkanen, J., Peräkylä, O., Lehtipalo, K., Hussein,
582 T., Petäjä, T., Kerminen, V. M., Bäck, J., and Kulmala, M.: Long-term analysis of clear-sky new particle formation
583 events and nonevents in Hyytiälä, Atmos. Chem. Phys., 17, 6227-6241, 10.5194/acp-17-6227-2017, 2017.
584
585 Donahue, N. M., Ortega, I. K., Chuang, W., Riipinen, I., Riccobono, F., Schobesberger, S., Dommen, J.,
586 Baltensperger, U., Kulmala, M., Worsnop, D. R., and Vehkamaki, H.: How do organic vapors contribute to new-
587 particle formation?, Faraday Discussions, 165, 91-104, 10.1039/C3FD00046J, 2013.
588
589 Drewnick, F., Hings, S. S., DeCarlo, P., Jayne, J. T., Gonin, M., Fuhrer, K., Weimer, S., Jimenez, J. L., Demerjian,
590 K. L., Borrmann, S., and Worsnop, D. R.: A New Time-of-Flight Aerosol Mass Spectrometer (TOF-AMS)—
591 Instrument Description and First Field Deployment, Aerosol Science and Technology, 39, 637-658,
592 10.1080/02786820500182040, 2005.
593
594 Ehn, M., Junninen, H., Petäjä, T., Kurtén, T., Kerminen, V. M., Schobesberger, S., Manninen, H. E., Ortega, I. K.,
595 Vehkamäki, H., Kulmala, M., and Worsnop, D. R.: Composition and temporal behavior of ambient ions in the
596 boreal forest, Atmos. Chem. Phys., 10, 8513-8530, 10.5194/acp-10-8513-2010, 2010.
597
598 Ehn, M., Kleist, E., Junninen, H., Petäjä, T., Lönn, G., Schobesberger, S., Dal Maso, M., Trimborn, A., Kulmala,
599 M., Worsnop, D. R., Wahner, A., Wildt, J., and Mentel, T. F.: Gas phase formation of extremely oxidized pinene
600 reaction products in chamber and ambient air, Atmos. Chem. Phys., 12, 5113-5127, 10.5194/acp-12-5113-2012,
601 2012.
602
603 Ehn, M., Thornton, J. A., Kleist, E., Sipilä, M., Junninen, H., Pullinen, I., Springer, M., Rubach, F., Tillmann, R.,
604 Lee, B., Lopez-Hilfiker, F., Andres, S., Acir, I.-H., Rissanen, M., Jokinen, T., Schobesberger, S., Kangasluoma, J.,
605 Kontkanen, J., Nieminen, T., Kurtén, T., Nielsen, L. B., Jørgensen, S., Kjaergaard, H. G., Canagaratna, M., Maso,
606 M. D., Berndt, T., Petäjä, T., Wahner, A., Kerminen, V.-M., Kulmala, M., Worsnop, D. R., Wildt, J., and Mentel,
607 T. F.: A large source of low-volatility secondary organic aerosol, Nature, 506, 476-479, 10.1038/nature13032, 2014.
608
609 Garmash, O., Rissanen, M. P., Pullinen, I., Schmitt, S., Kausiala, O., Tillmann, R., Zhao, D., Percival, C., Bannan,
610 T. J., Priestley, M., Hallquist, A. M., Kleist, E., Kiendler-Scharr, A., Hallquist, M., Berndt, T., McFiggans, G.,
611 Wildt, J., Mentel, T., and Ehn, M.: Multi-generation OH oxidation as a source for highly oxygenated organic
612 molecules from aromatics, Atmospheric Chemistry and Physics, 20, 515-537, 10.5194/acp-20-515-2020, 2020.
613
614 Gordon, H., Kirkby, J., Baltensperger, U., Bianchi, F., Breitenlechner, M., Curtius, J., Dias, A., Dommen, J.,
615 Donahue, N. M., Dunne, E. M., Duplissy, J., Ehrhart, S., Flagan, R. C., Frege, C., Fuchs, C., Hansel, A., Hoyle, C.
616 R., Kulmala, M., Kürten, A., Lehtipalo, K., Makhmutov, V., Molteni, U., Rissanen, M. P., Stozhkov, Y., Tröstl, J.,
617 Tsagkogeorgas, G., Wagner, R., Williamson, C., Wimmer, D., Winkler, P. M., Yan, C., and Carslaw, K. S.: Causes

618   and importance of new particle formation in the present-day and preindustrial atmospheres, Journal of Geophysical
619   Research: Atmospheres, 122, 8739-8760, https://doi.org/10.1002/2017JD026844, 2017.
620
621   Guo, Y., Yan, C., Li, C., Ma, W., Feng, Z., Zhou, Y., Lin, Z., Dada, L., Stolzenburg, D., Yin, R., Kontkanen, J.,
622   Daellenbach, K. R., Kangasluoma, J., Yao, L., Chu, B., Wang, Y., Cai, R., Bianchi, F., Liu, Y., and Kulmala, M.:
623   Formation of nighttime sulfuric acid from the ozonolysis of alkenes in Beijing, Atmos. Chem. Phys., 21, 5499-5511,
624   10.5194/acp-21-5499-2021, 2021.
625
626   Hallquist, M., Wenger, J. C., Baltensperger, U., Rudich, Y., Simpson, D., Claeys, M., Dommen, J., Donahue, N.
627   M., George, C., Goldstein, A. H., Hamilton, J. F., Herrmann, H., Hoffmann, T., Iinuma, Y., Jang, M., Jenkin, M.
628   E., Jimenez, J. L., Kiendler-Scharr, A., Maenhaut, W., McFiggans, G., Mentel, T. F., Monod, A., Prevot, A. S. H.,
629   Seinfeld, J. H., Surratt, J. D., Szmigielski, R., and Wildt, J.: The formation, properties and impact of secondary
630   organic aerosol: current and emerging issues, Atmospheric Chemistry and Physics, 9, 5155-5236, 10.5194/acp-9-
631   5155-2009, 2009.
632
633   Heinritzi, M., Simon, M., Steiner, G., Wagner, A. C., Kürten, A., Hansel, A., and Curtius, J.: Characterization of
634   the mass-dependent transmission efficiency of a CIMS, Atmos. Meas. Tech., 9, 1449-1460, 10.5194/amt-9-1449-
635   2016, 2016.
636
637   Heinritzi, M., Dada, L., Simon, M., Stolzenburg, D., Wagner, A. C., Fischer, L., Ahonen, L. R., Amanatidis, S.,
638   Baalbaki, R., Baccarini, A., Bauer, P. S., Baumgartner, B., Bianchi, F., Brilke, S., Chen, D., Chiu, R., Dias, A.,
639   Dommen, J., Duplissy, J., Finkenzeller, H., Frege, C., Fuchs, C., Garmash, O., Gordon, H., Granzin, M., El Haddad,
640   I., He, X., Helm, J., Hofbauer, V., Hoyle, C. R., Kangasluoma, J., Keber, T., Kim, C., Kürten, A., Lamkaddam, H.,
641   Laurila, T. M., Lampilahti, J., Lee, C. P., Lehtipalo, K., Leiminger, M., Mai, H., Makhmutov, V., Manninen, H. E.,
642   Marten, R., Mathot, S., Mauldin, R. L., Mentler, B., Molteni, U., Müller, T., Nie, W., Nieminen, T., Onnela, A.,
643   Partoll, E., Passananti, M., Petäjä, T., Pfeifer, J., Pospisilova, V., Quéléver, L. L. J., Rissanen, M. P., Rose, C.,
644   Schobesberger, S., Scholz, W., Scholze, K., Sipilä, M., Steiner, G., Stozhkov, Y., Tauber, C., Tham, Y. J., Vazquez-
645   Pufleau, M., Virtanen, A., Vogel, A. L., Volkamer, R., Wagner, R., Wang, M., Weitz, L., Wimmer, D., Xiao, M.,
646   Yan, C., Ye, P., Zha, Q., Zhou, X., Amorim, A., Baltensperger, U., Hansel, A., Kulmala, M., Tomé, A., Winkler,
647   P. M., Worsnop, D. R., Donahue, N. M., Kirkby, J., and Curtius, J.: Molecular understanding of the suppression of
648   new-particle formation by isoprene, Atmos. Chem. Phys., 20, 11809-11821, 10.5194/acp-20-11809-2020, 2020.
649
650   Huang, W., Li, H., Sarnela, N., Heikkinen, L., Tham, Y. J., Mikkilä, J., Thomas, S. J., Donahue, N. M., Kulmala,
651   M., and Bianchi, F.: Measurement report: Molecular composition and volatility of gaseous organic compounds in
652   a boreal forest: from volatile organic compounds to highly oxygenated organic molecules, Atmos. Chem. Phys.
653   Discuss., 2020, 1-27, 10.5194/acp-2020-1257, 2020.
654
655   Hyttinen, N., Kupiainen-Määttä, O., Rissanen, M. P., Muuronen, M., Ehn, M., and Kurtén, T.: Modeling the
656   Charging of Highly Oxidized Cyclohexene Ozonolysis Products Using Nitrate-Based Chemical Ionization, The
657   Journal of Physical Chemistry A, 119, 6339-6345, 10.1021/acs.jpca.5b01818, 2015.
658

659 Hyttinen, N., Otkjær, R. V., Iyer, S., Kjaergaard, H. G., Rissanen, M. P., Wennberg, P. O., and Kurtén, T.:
660 Computational Comparison of Different Reagent Ions in the Chemical Ionization of Oxidized Multifunctional
661 Compounds, The Journal of Physical Chemistry A, 122, 269-279, 10.1021/acs.jpca.7b10015, 2018.

663 Jayne, J. T., Leard, D. C., Zhang, X., Davidovits, P., Smith, K. A., Kolb, C. E., and Worsnop, D. R.: Development
664 of an Aerosol Mass Spectrometer for Size and Composition Analysis of Submicron Particles, Aerosol Science and
665 Technology, 33, 49-70, 10.1080/027868200410840, 2000.

667 Jimenez, J. L., Canagaratna, M. R., Donahue, N. M., Prevot, A. S. H., Zhang, Q., Kroll, J. H., DeCarlo, P. F., Allan,
668 J. D., Coe, H., Ng, N. L., Aiken, A. C., Docherty, K. S., Ulbrich, I. M., Grieshop, A. P., Robinson, A. L., Duplissy,
669 J., Smith, J. D., Wilson, K. R., Lanz, V. A., Hueglin, C., Sun, Y. L., Tian, J., Laaksonen, A., Raatikainen, T.,
670 Rautiainen, J., Vaattovaara, P., Ehn, M., Kulmala, M., Tomlinson, J. M., Collins, D. R., Cubison, M. J., Dunlea, J.,
671 Huffman, J. A., Onasch, T. B., Alfarra, M. R., Williams, P. I., Bower, K., Kondo, Y., Schneider, J., Drewnick, F.,
672 Borrmann, S., Weimer, S., Demerjian, K., Salcedo, D., Cottrell, L., Griffin, R., Takami, A., Miyoshi, T.,
673 Hatakeyama, S., Shimono, A., Sun, J. Y., Zhang, Y. M., Dzepina, K., Kimmel, J. R., Sueper, D., Jayne, J. T.,
674 Herndon, S. C., Trimborn, A. M., Williams, L. R., Wood, E. C., Middlebrook, A. M., Kolb, C. E., Baltensperger,
675 U., and Worsnop, D. R.: Evolution of Organic Aerosols in the Atmosphere, Science, 326, 1525,
676 10.1126/science.1180353, 2009.

678 Jokinen, T., Sipilä, M., Junninen, H., Ehn, M., Lönn, G., Hakala, J., Petäjä, T., Mauldin Iii, R. L., Kulmala, M., and
679 Worsnop, D. R.: Atmospheric sulphuric acid and neutral cluster measurements using CI-APi-TOF, Atmos. Chem.
680 Phys., 12, 4117-4125, 10.5194/acp-12-4117-2012, 2012.

682 Jokinen, T., Sipilä, M., Richters, S., Kerminen, V.-M., Paasonen, P., Stratmann, F., Worsnop, D., Kulmala, M., Ehn,
683 M., Herrmann, H., and Berndt, T.: Rapid Autoxidation Forms Highly Oxidized RO2 Radicals in the Atmosphere,
684 Angewandte Chemie International Edition, 53, 14596-14600, https://doi.org/10.1002/anie.201408566, 2014.

686 Junninen, H., Ehn, M., Petäjä, T., Luosujärvi, L., Kotiaho, T., Kostiainen, R., Rohner, U., Gonin, M., Fuhrer, K.,
687 Kulmala, M., and Worsnop, D. R.: A high-resolution mass spectrometer to measure atmospheric ion composition,
688 Atmos. Meas. Tech., 3, 1039-1053, 10.5194/amt-3-1039-2010, 2010.

690 Kirkby, J., Duplissy, J., Sengupta, K., Frege, C., Gordon, H., Williamson, C., Heinritzi, M., Simon, M., Yan, C.,
691 Almeida, J., Tröstl, J., Nieminen, T., Ortega, I. K., Wagner, R., Adamov, A., Amorim, A., Bernhammer, A.-K.,
692 Bianchi, F., Breitenlechner, M., Brilke, S., Chen, X., Craven, J., Dias, A., Ehrhart, S., Flagan, R. C., Franchin, A.,
693 Fuchs, C., Guida, R., Hakala, J., Hoyle, C. R., Jokinen, T., Junninen, H., Kangasluoma, J., Kim, J., Krapf, M.,
694 Kürten, A., Laaksonen, A., Lehtipalo, K., Makhmutov, V., Mathot, S., Molteni, U., Onnela, A., Peräkylä, O., Piel,
695 F., Petäjä, T., Praplan, A. P., Pringle, K., Rap, A., Richards, N. A. D., Riipinen, I., Rissanen, M. P., Rondo, L.,
696 Sarnela, N., Schobesberger, S., Scott, C. E., Seinfeld, J. H., Sipilä, M., Steiner, G., Stozhkov, Y., Stratmann, F.,
697 Tomé, A., Virtanen, A., Vogel, A. L., Wagner, A. C., Wagner, P. E., Weingartner, E., Wimmer, D., Winkler, P. M.,
698 Ye, P., Zhang, X., Hansel, A., Dommen, J., Donahue, N. M., Worsnop, D. R., Baltensperger, U., Kulmala, M.,
699 Carslaw, K. S., and Curtius, J.: Ion-induced nucleation of pure biogenic particles, Nature, 533, 521-526,
700 10.1038/nature17953, 2016.

701

702 Krechmer, J. E., Coggon, M. M., Massoli, P., Nguyen, T. B., Crounse, J. D., Hu, W., Day, D. A., Tyndall, G. S.,
703 Henze, D. K., Rivera-Rios, J. C., Nowak, J. B., Kimmel, J. R., Mauldin, R. L., Stark, H., Jayne, J. T., Sipilä, M.,
704 Junninen, H., St. Clair, J. M., Zhang, X., Feiner, P. A., Zhang, L., Miller, D. O., Brune, W. H., Keutsch, F. N.,
705 Wennberg, P. O., Seinfeld, J. H., Worsnop, D. R., Jimenez, J. L., and Canagaratna, M. R.: Formation of Low
706 Volatility Organic Compounds and Secondary Organic Aerosol from Isoprene Hydroxyhydroperoxide Low-NO
707 Oxidation, Environmental Science & Technology, 49, 10330-10339, 10.1021/acs.est.5b02031, 2015.

708

709 Kulmala, M., Kontkanen, J., Junninen, H., Lehtipalo, K., Manninen, H. E., Nieminen, T., Petäjä, T., Sipilä, M.,
710 Schobesberger, S., Rantala, P., Franchin, A., Jokinen, T., Järvinen, E., Äijälä, M., Kangasluoma, J., Hakala, J.,
711 Aalto, P. P., Paasonen, P., Mikkilä, J., Vanhanen, J., Aalto, J., Hakola, H., Makkonen, U., Ruuskanen, T., Mauldin,
712 R. L., 3rd, Duplissy, J., Vehkamäki, H., Bäck, J., Kortelainen, A., Riipinen, I., Kurtén, T., Johnston, M. V., Smith,
713 J. N., Ehn, M., Mentel, T. F., Lehtinen, K. E., Laaksonen, A., Kerminen, V. M., and Worsnop, D. R.: Direct
714 observations of atmospheric aerosol nucleation, Science, 339, 943-946, 10.1126/science.1227385, 2013.

715

716 Kürten, A., Bergen, A., Heinritzi, M., Leiminger, M., Lorenz, V., Piel, F., Simon, M., Sitals, R., Wagner, A. C.,
717 and Curtius, J.: Observation of new particle formation and measurement of sulfuric acid, ammonia, amines and
718 highly oxidized organic molecules at a rural site in central Germany, Atmos. Chem. Phys., 16, 12793-12813,
719 10.5194/acp-16-12793-2016, 2016.

720

721 Le Breton, M., Wang, Y., Hallquist, Å. M., Pathak, R. K., Zheng, J., Yang, Y., Shang, D., Glasius, M., Bannan, T.
722 J., Liu, Q., Chan, C. K., Percival, C. J., Zhu, W., Lou, S., Topping, D., Wang, Y., Yu, J., Lu, K., Guo, S., Hu, M.,
723 and Hallquist, M.: Online gas- and particle-phase measurements of organosulfates, organosulfonates and nitrooxy
724 organosulfates in Beijing utilizing a FIGAERO ToF-CIMS, Atmos. Chem. Phys., 18, 10355-10371, 10.5194/acp-
725 18-10355-2018, 2018.

726

727 Lehtipalo, K., Yan, C., Dada, L., Bianchi, F., Xiao, M., Wagner, R., Stolzenburg, D., Ahonen, L., Amorim, A.,
728 Baccarini, A., Bauer, P., Baumgartner, B., Bergen, A., Bernhammer, A.-K., Breitenlechner, M., Brilke, S., Buchholz,
729 A., Mazon, S., Chen, D., and Worsnop, D.: Multicomponent new particle formation from sulfuric acid, ammonia,
730 and biogenic vapors, Science Advances, 4, eaau5363, 10.1126/sciadv.aau5363, 2018.

731

732 Lelieveld, J., Evans, J. S., Fnais, M., Giannadaki, D., and Pozzer, A.: The contribution of outdoor air pollution
733 sources to premature mortality on a global scale, Nature, 525, 367-371, 10.1038/nature15371, 2015.

734

735 Liu, Y., Yan, C., Feng, Z., Zheng, F., Fan, X., Zhang, Y., Li, C., Zhou, Y., Lin, Z., Guo, Y., Zhang, Y., Ma, L.,
736 Zhou, W., Liu, Z., Dada, L., Dällenbach, K., Kontkanen, J., Cai, R., Chan, T., Chu, B., Du, W., Yao, L., Wang, Y.,
737 Cai, J., Kangasluoma, J., Kokkonen, T., Kujansuu, J., Rusanen, A., Deng, C., Fu, Y., Yin, R., Li, X., Lu, Y., Liu,
738 Y., Lian, C., Yang, D., Wang, W., Ge, M., Wang, Y., Worsnop, D. R., Junninen, H., He, H., Kerminen, V.-M.,
739 Zheng, J., Wang, L., Jiang, J., Petäjä, T., Bianchi, F., and Kulmala, M.: Continuous and comprehensive atmospheric
740 observations in Beijing: a station to understand the complex urban atmospheric environment, Big Earth Data, 4,
741 295-321, 10.1080/20964471.2020.1798707, 2020.

742

743   Liu, Y., Nie, W., Li, Y., Ge, D., Liu, C., Xu, Z., Chen, L., Wang, T., Wang, L., Sun, P., Qi, X., Wang, J., Xu, Z.,
744   Yuan, J., Yan, C., Zhang, Y., Huang, D., Wang, Z., Donahue, N. M., Worsnop, D., Chi, X., Ehn, M., and Ding, A.:
745   Formation of condensable organic vapors from anthropogenic and biogenic VOCs is strongly perturbed by NOx in
746   eastern China, Atmos. Chem. Phys. Discuss., 2021, 1-44, 10.5194/acp-2021-364, 2021.

748   Massoli, P., Stark, H., Canagaratna, M. R., Krechmer, J. E., Xu, L., Ng, N. L., Mauldin, R. L., Yan, C., Kimmel, J.,
749   Misztal, P. K., Jimenez, J. L., Jayne, J. T., and Worsnop, D. R.: Ambient Measurements of Highly Oxidized Gas-
750   Phase Molecules during the Southern Oxidant and Aerosol Study (SOAS) 2013, ACS Earth and Space Chemistry,
751   2, 653-672, 10.1021/acsearthspacechem.8b00028, 2018.

753   Mehra, A., Canagaratna, M., Bannan, T. J., Worrall, S. D., Bacak, A., Priestley, M., Liu, D., Zhao, J., Xu, W., Sun,
754   Y., Hamilton, J. F., Squires, F. A., Lee, J., Bryant, D. J., Hopkins, J. R., Elzein, A., Budisulistiorini, S. H., Cheng,
755   X., Chen, Q., Wang, Y., Wang, L., Stark, H., Krechmer, J. E., Brean, J., Slater, E., Whalley, L., Heard, D., Ouyang,
756   B., Acton, W. J. F., Hewitt, C. N., Wang, X., Fu, P., Jayne, J., Worsnop, D., Allan, J., Percival, C., and Coe, H.:
757   Using highly time-resolved online mass spectrometry to examine biogenic and anthropogenic contributions to
758   organic aerosol in Beijing, Faraday Discussions, 10.1039/D0FD00080A, 2021.

760   Merikanto, J., Spracklen, D. V., Mann, G. W., Pickering, S. J., and Carslaw, K. S.: Impact of nucleation on global
761   CCN, Atmos. Chem. Phys., 9, 8601-8616, 10.5194/acp-9-8601-2009, 2009.

763   Mo, Z., Shao, M., Wang, W., Liu, Y., Wang, M., and Lu, S.: Evaluation of biogenic isoprene emissions and their
764   contribution to ozone formation by ground-based measurements in Beijing, China, Science of The Total
765   Environment, 627, 1485-1494, https://doi.org/10.1016/j.scitotenv.2018.01.336, 2018.

767   Mohr, C., Thornton, J. A., Heitto, A., Lopez-Hilfiker, F. D., Lutz, A., Riipinen, I., Hong, J., Donahue, N. M.,
768   Hallquist, M., Petäjä, T., Kulmala, M., and Yli-Juuti, T.: Molecular identification of organic vapors driving
769   atmospheric nanoparticle growth, Nature Communications, 10, 4442, 10.1038/s41467-019-12473-2, 2019.

771   Molteni, U., Bianchi, F., Klein, F., El Haddad, I., Frege, C., Rossi, M. J., Dommen, J., and Baltensperger, U.:
772   Formation of highly oxygenated organic molecules from aromatic compounds, Atmos. Chem. Phys., 18, 1909-1921,
773   10.5194/acp-18-1909-2018, 2018.

775   Mutzel, A., Poulain, L., Berndt, T., Iinuma, Y., Rodigast, M., Böge, O., Richters, S., Spindler, G., Sipilä, M.,
776   Jokinen, T., Kulmala, M., and Herrmann, H.: Highly Oxidized Multifunctional Organic Compounds Observed in
777   Tropospheric Particles: A Field and Laboratory Study, Environmental Science & Technology, 49, 7754-7761,
778   10.1021/acs.est.5b00885, 2015.

780   Nah, T., Sanchez, J., Boyd, C., and Ng, N.: Photochemical Aging of α-pinene and β-pinene Secondary Organic
781   Aerosol   formed   from   Nitrate   Radical   Oxidation,   Environmental   Science   &   Technology,   50,
782   10.1021/acs.est.5b04594, 2015.

783

Atmospheric
Chemistry
and Physics
Discussions

784   Nie, W., Yan, C., Huang, D., Wang, Z., and et al.: Secondary organic aerosol formed by condensing anthropogenic
785   vapors over China's megacities (accepted), Nature Geoscience, 2022.
786
787   O'Dowd, C. D., Aalto, P., Hmeri, K., Kulmala, M., and Hoffmann, T.: Atmospheric particles from organic vapours,
788   Nature, 416, 497-498, 10.1038/416497a, 2002.
789
790   Orlando, J. J., and Tyndall, G. S.: Laboratory studies of organic peroxy radical chemistry: an overview with
791   emphasis on recent issues of atmospheric significance, Chemical Society Reviews, 41, 6294-6317,
792   10.1039/C2CS35166H, 2012.
793
794   Pan, S., and Wang, L.: Atmospheric Oxidation Mechanism of m-Xylene Initiated by OH Radical, The Journal of
795   Physical Chemistry A, 118, 10778-10787, 10.1021/jp506815v, 2014.
796
797   Panopoulou, A., Liakakou, E., Sauvage, S., Gros, V., Locoge, N., Stavroulas, I., Bonsang, B., Gerasopoulos, E.,
798   and Mihalopoulos, N.: Yearlong measurements of monoterpenes and isoprene in a Mediterranean city (Athens):
799   Natural   vs   anthropogenic   origin,   Atmospheric   Environment,   243,   117803,
800   https://doi.org/10.1016/j.atmosenv.2020.117803, 2020.
801
802   Riccobono, F., Schobesberger, S., Scott, C., Dommen, J., Ortega, I., Rondo, L., Almeida, J., Amorim, A., Bianchi,
803   F., Breitenlechner, M., David, A., Downard, A., Dunne, E., Duplissy, J., Ehrhart, S., Flagan, R., Franchin, A.,
804   Hansel, A., Junninen, H., and Baltensperger, U.: Oxidation Products of Biogenic Emissions Contribute to
805   Nucleation of Atmospheric Particles, Science (New York, N.Y.), 344, 717-721, 10.1126/science.1243527, 2014.
806
807   Riva, M., Rantala, P., Krechmer, J. E., Peräkylä, O., Zhang, Y., Heikkinen, L., Garmash, O., Yan, C., Kulmala, M.,
808   Worsnop, D., and Ehn, M.: Evaluating the performance of five different chemical ionization techniques for
809   detecting gaseous oxygenated organic species, Atmos. Meas. Tech., 12, 2403-2421, 10.5194/amt-12-2403-2019,
810   2019.
811
812   Roldin, P., Ehn, M., Kurtén, T., Olenius, T., Rissanen, M. P., Sarnela, N., Elm, J., Rantala, P., Hao, L., Hyttinen,
813   N., Heikkinen, L., Worsnop, D. R., Pichelstorfer, L., Xavier, C., Clusius, P., Öström, E., Petäjä, T., Kulmala, M.,
814   Vehkamäki, H., Virtanen, A., Riipinen, I., and Boy, M.: The role of highly oxygenated organic molecules in the
815   Boreal aerosol-cloud-climate system, Nature Communications, 10, 4370, 10.1038/s41467-019-12338-8, 2019.
816
817   Rose, C., Zha, Q., Dada, L., Yan, C., Lehtipalo, K., Junninen, H., Mazon, S. B., Jokinen, T., Sarnela, N., Sipilä, M.,
818   Petäjä, T., Kerminen, V.-M., Bianchi, F., and Kulmala, M.: Observations of biogenic ion-induced cluster formation
819   in the atmosphere, Science Advances, 4, eaar5218, 10.1126/sciadv.aar5218, 2018.
820
821   Schervish, M., and Donahue, N. M.: Peroxy radical chemistry and the volatility basis set, Atmos. Chem. Phys., 20,
822   1183-1199, 10.5194/acp-20-1183-2020, 2020.
823
824   Schobesberger, S., Junninen, H., Bianchi, F., Lönn, G., Ehn, M., Lehtipalo, K., Dommen, J., Ehrhart, S., Ortega, I.
825   K., Franchin, A., Nieminen, T., Riccobono, F., Hutterli, M., Duplissy, J., Almeida, J., Amorim, A., Breitenlechner,

826 M., Downard, A. J., Dunne, E. M., Flagan, R. C., Kajos, M., Keskinen, H., Kirkby, J., Kupc, A., Kürten, A., Kurtén,
827 T., Laaksonen, A., Mathot, S., Onnela, A., Praplan, A. P., Rondo, L., Santos, F. D., Schallhart, S., Schnitzhofer, R.,
828 Sipilä, M., Tomé, A., Tsagkogeorgas, G., Vehkamäki, H., Wimmer, D., Baltensperger, U., Carslaw, K. S., Curtius,
829 J., Hansel, A., Petäjä, T., Kulmala, M., Donahue, N. M., and Worsnop, D. R.: Molecular understanding of
830 atmospheric particle formation from sulfuric acid and large oxidized organic molecules, Proceedings of the National
831 Academy of Sciences, 110, 17223, 10.1073/pnas.1306973110, 2013.

833 Seinfeld, J. H., and Pandis, S. N.: Atmospheric chemistry and physics: from air pollution to climate change, John
834 Wiley & Sons, 2016.

836 Song, K., Guo, S., Wang, H., Yu, Y., Wang, H., Tang, R., Xia, S., Gong, Y., Wan, Z., Lv, D., Tan, R., Zhu, W.,
837 Shen, R., Li, X., Yu, X., Chen, S., Zeng, L., and Huang, X.: Measurement Report: Online Measurement of Gas-
838 Phase Nitrated Phenols Utilizing CI-LToF-MS: Primary Sources and Secondary Formation, Atmos. Chem. Phys.
839 Discuss., 2021, 1-28, 10.5194/acp-2020-1294, 2021.

841 Stocker, T.: Climate change 2013: the physical science basis: Working Group I contribution to the Fifth assessment
842 report of the Intergovernmental Panel on Climate Change, 2014.

844 Stolzenburg, D., Fischer, L., Vogel, A. L., Heinritzi, M., Schervish, M., Simon, M., Wagner, A. C., Dada, L.,
845 Ahonen, L. R., Amorim, A., Baccarini, A., Bauer, P. S., Baumgartner, B., Bergen, A., Bianchi, F., Breitenlechner,
846 M., Brilke, S., Buenrostro Mazon, S., Chen, D., Dias, A., Draper, D. C., Duplissy, J., El Haddad, I., Finkenzeller,
847 H., Frege, C., Fuchs, C., Garmash, O., Gordon, H., He, X., Helm, J., Hofbauer, V., Hoyle, C. R., Kim, C., Kirkby,
848 J., Kontkanen, J., Kürten, A., Lampilahti, J., Lawler, M., Lehtipalo, K., Leiminger, M., Mai, H., Mathot, S., Mentler,
849 B., Molteni, U., Nie, W., Nieminen, T., Nowak, J. B., Ojdanic, A., Onnela, A., Passananti, M., Petäjä, T., Quéléver,
850 L. L. J., Rissanen, M. P., Sarnela, N., Schallhart, S., Tauber, C., Tomé, A., Wagner, R., Wang, M., Weitz, L.,
851 Wimmer, D., Xiao, M., Yan, C., Ye, P., Zha, Q., Baltensperger, U., Curtius, J., Dommen, J., Flagan, R. C., Kulmala,
852 M., Smith, J. N., Worsnop, D. R., Hansel, A., Donahue, N. M., and Winkler, P. M.: Rapid growth of organic aerosol
853 nanoparticles over a wide tropospheric temperature range, Proceedings of the National Academy of Sciences, 115,
854 9122, 10.1073/pnas.1807604115, 2018.

856 Teng, A. P., Crounse, J. D., and Wennberg, P. O.: Isoprene Peroxy Radical Dynamics, Journal of the American
857 Chemical Society, 139, 5367-5377, 10.1021/jacs.6b12838, 2017.

859 Tröstl, J., Chuang, W. K., Gordon, H., Heinritzi, M., Yan, C., Molteni, U., Ahlm, L., Frege, C., Bianchi, F., Wagner,
860 R., Simon, M., Lehtipalo, K., Williamson, C., Craven, J. S., Duplissy, J., Adamov, A., Almeida, J., Bernhammer,
861 A.-K., Breitenlechner, M., Brilke, S., Dias, A., Ehrhart, S., Flagan, R. C., Franchin, A., Fuchs, C., Guida, R., Gysel,
862 M., Hansel, A., Hoyle, C. R., Jokinen, T., Junninen, H., Kangasluoma, J., Keskinen, H., Kim, J., Krapf, M., Kürten,
863 A., Laaksonen, A., Lawler, M., Leiminger, M., Mathot, S., Möhler, O., Nieminen, T., Onnela, A., Petäjä, T., Piel,
864 F. M., Miettinen, P., Rissanen, M. P., Rondo, L., Sarnela, N., Schobesberger, S., Sengupta, K., Sipilä, M., Smith, J.
865 N., Steiner, G., Tomè, A., Virtanen, A., Wagner, A. C., Weingartner, E., Wimmer, D., Winkler, P. M., Ye, P.,
866 Carslaw, K. S., Curtius, J., Dommen, J., Kirkby, J., Kulmala, M., Riipinen, I., Worsnop, D. R., Donahue, N. M.,

Atmospheric
Chemistry
and Physics
Discussions

867   and Baltensperger, U.: The role of low-volatility organic compounds in initial particle growth in the atmosphere,
868   Nature, 533, 527-531, 10.1038/nature18271, 2016.

869

870   Wagner, P., and Kuttler, W.: Biogenic and anthropogenic isoprene in the near-surface urban atmosphere — A case
871   study   in   Essen,   Germany,   Science   of   The   Total   Environment,   475,   104-115,
872   https://doi.org/10.1016/j.scitotenv.2013.12.026, 2014.

873

874   Wang, H., Lu, K., Guo, S., Wu, Z., Shang, D., Tan, Z., Wang, Y., Le Breton, M., Lou, S., Tang, M., Wu, Y., Zhu,
875   W., Zheng, J., Zeng, L., Hallquist, M., Hu, M., and Zhang, Y.: Efficient N2O5 uptake and NO3 oxidation in the
876   outflow of urban Beijing, Atmos. Chem. Phys., 18, 9705-9721, 10.5194/acp-18-9705-2018, 2018a.

877

878   Wang, S., Wu, R., Berndt, T., Ehn, M., and Wang, L.: Formation of Highly Oxidized Radicals and Multifunctional
879   Products from the Atmospheric Oxidation of Alkylbenzenes, Environmental Science & Technology, 51, 8442-8449,
880   10.1021/acs.est.7b02374, 2017.

881

882   Wang, S., Riva, M., Yan, C., Ehn, M., and Wang, L.: Primary Formation of Highly Oxidized Multifunctional
883   Products in the OH-Initiated Oxidation of Isoprene: A Combined Theoretical and Experimental Study,
884   Environmental Science & Technology, 52, 12255-12264, 10.1021/acs.est.8b02783, 2018b.

885

886   Wang, Y., Hu, M., Wang, Y., Zheng, J., Shang, D., Yang, Y., Liu, Y., Li, X., Tang, R., Zhu, W., Du, Z., Wu, Y.,
887   Guo, S., Wu, Z., Lou, S., Hallquist, M., and Yu, J. Z.: The formation of nitro-aromatic compounds under high NOx
888   and anthropogenic VOC conditions in urban Beijing, China, Atmos. Chem. Phys., 19, 7649-7665, 10.5194/acp-19-
889   7649-2019, 2019.

890

891   Wu, R., Vereecken, L., Tsiligiannis, E., Kang, S., Albrecht, S. R., Hantschke, L., Zhao, D., Novelli, A., Fuchs, H.,
892   Tillmann, R., Hohaus, T., Carlsson, P. T. M., Shenolikar, J., Bernard, F., Crowley, J. N., Fry, J. L., Brownwood, B.,
893   Thornton, J. A., Brown, S. S., Kiendler-Scharr, A., Wahner, A., Hallquist, M., and Mentel, T. F.: Molecular
894   composition and volatility of multi-generation products formed from isoprene oxidation by nitrate radical, Atmos.
895   Chem. Phys., 21, 10799-10824, 10.5194/acp-21-10799-2021, 2021.

896

897   Xu, L., Møller, K. H., Crounse, J. D., Kjaergaard, H. G., and Wennberg, P. O.: New Insights into the Radical
898   Chemistry and Product Distribution in the OH-Initiated Oxidation of Benzene, Environmental Science &
899   Technology, 54, 13467-13477, 10.1021/acs.est.0c04780, 2020.

900

901   Xu, Z. N., Nie, W., Liu, Y. L., Sun, P., Huang, D. D., Yan, C., Krechmer, J., Ye, P. L., Xu, Z., Qi, X. M., Zhu, C.
902   J., Li, Y. Y., Wang, T. Y., Wang, L., Huang, X., Tang, R. Z., Guo, S., Xiu, G. L., Fu, Q. Y., Worsnop, D., Chi, X.
903   G., and Ding, A. J.: Multifunctional Products of Isoprene Oxidation in Polluted Atmosphere and Their Contribution
904   to SOA, Geophysical Research Letters, 48, e2020GL089276, https://doi.org/10.1029/2020GL089276, 2021.

905

906   Yan, C., Nie, W., Äijälä, M., Rissanen, M. P., Canagaratna, M. R., Massoli, P., Junninen, H., Jokinen, T., Sarnela,
907   N., Häme, S. A. K., Schobesberger, S., Canonaco, F., Yao, L., Prévôt, A. S. H., Petäjä, T., Kulmala, M., Sipilä, M.,
908   Worsnop, D. R., and Ehn, M.: Source characterization of highly oxidized multifunctional compounds in a boreal

909 forest environment using positive matrix factorization, Atmos. Chem. Phys., 16, 12715-12731, 10.5194/acp-16-
910 12715-2016, 2016.

911

912 Yan, C., Nie, W., Vogel, A. L., Dada, L., Lehtipalo, K., Stolzenburg, D., Wagner, R., Rissanen, M. P., Xiao, M.,
913 Ahonen, L., Fischer, L., Rose, C., Bianchi, F., Gordon, H., Simon, M., Heinritzi, M., Garmash, O., Roldin, P., Dias,
914 A., Ye, P., Hofbauer, V., Amorim, A., Bauer, P. S., Bergen, A., Bernhammer, A. K., Breitenlechner, M., Brilke, S.,
915 Buchholz, A., Mazon, S. B., Canagaratna, M. R., Chen, X., Ding, A., Dommen, J., Draper, D. C., Duplissy, J.,
916 Frege, C., Heyn, C., Guida, R., Hakala, J., Heikkinen, L., Hoyle, C. R., Jokinen, T., Kangasluoma, J., Kirkby, J.,
917 Kontkanen, J., Kürten, A., Lawler, M. J., Mai, H., Mathot, S., Mauldin, R. L., Molteni, U., Nichman, L., Nieminen,
918 T., Nowak, J., Ojdanic, A., Onnela, A., Pajunoja, A., Petäjä, T., Piel, F., Quéléver, L. L. J., Sarnela, N., Schallhart,
919 S., Sengupta, K., Sipilä, M., Tomé, A., Tröstl, J., Väisänen, O., Wagner, A. C., Ylisirniö, A., Zha, Q., Baltensperger,
920 U., Carslaw, K. S., Curtius, J., Flagan, R. C., Hansel, A., Riipinen, I., Smith, J. N., Virtanen, A., Winkler, P. M.,
921 Donahue, N. M., Kerminen, V. M., Kulmala, M., Ehn, M., and Worsnop, D. R.: Size-dependent influence of
922 NO$_x$ on the growth rates of organic aerosol particles, Science Advances, 6, eaay4945,
923 10.1126/sciadv.aay4945, 2020.

924

925 Yan, C., Yin, R., Lu, Y., Dada, L., Yang, D., Fu, Y., Kontkanen, J., Deng, C., Garmash, O., Ruan, J., Baalbaki, R.,
926 Schervish, M., Cai, R., Bloss, M., Chan, T., Chen, T., Chen, Q., Chen, X., Chen, Y., Chu, B., Dällenbach, K.,
927 Foreback, B., He, X., Heikkinen, L., Jokinen, T., Junninen, H., Kangasluoma, J., Kokkonen, T., Kurppa, M.,
928 Lehtipalo, K., Li, H., Li, H., Li, X., Liu, Y., Ma, Q., Paasonen, P., Rantala, P., Pileci, R. E., Rusanen, A., Sarnela,
929 N., Simonen, P., Wang, S., Wang, W., Wang, Y., Xue, M., Yang, G., Yao, L., Zhou, Y., Kujansuu, J., Petäjä, T.,
930 Nie, W., Ma, Y., Ge, M., He, H., Donahue, N. M., Worsnop, D. R., Veli-Matti, K., Wang, L., Liu, Y., Zheng, J.,
931 Kulmala, M., Jiang, J., and Bianchi, F.: The Synergistic Role of Sulfuric Acid, Bases, and Oxidized Organics
932 Governing New-Particle Formation in Beijing, Geophysical Research Letters, 48, e2020GL091944,
933 https://doi.org/10.1029/2020GL091944, 2021.

934

935 Ye, C., Yuan, B., Lin, Y., Wang, Z., Hu, W., Li, T., Chen, W., Wu, C., Wang, C., Huang, S., Qi, J., Wang, B.,
936 Wang, C., Song, W., Wang, X., Zheng, E., Krechmer, J. E., Ye, P., Zhang, Z., Wang, X., Worsnop, D. R., and Shao,
937 M.: Chemical characterization of oxygenated organic compounds in gas-phase and particle-phase using iodide-
938 CIMS with FIGAERO in urban air, Atmos. Chem. Phys. Discuss., 2020, 1-62, 10.5194/acp-2020-1187, 2020.

939

940 Zaytsev, A., Koss, A. R., Breitenlechner, M., Krechmer, J. E., Nihill, K. J., Lim, C. Y., Rowe, J. C., Cox, J. L.,
941 Moss, J., Roscioli, J. R., Canagaratna, M. R., Worsnop, D. R., Kroll, J. H., and Keutsch, F. N.: Mechanistic study
942 of the formation of ring-retaining and ring-opening products from the oxidation of aromatic compounds under urban
943 atmospheric conditions, Atmos. Chem. Phys., 19, 15117-15129, 10.5194/acp-19-15117-2019, 2019.

944

945 Zha, Q., Yan, C., Junninen, H., Riva, M., Sarnela, N., Aalto, J., Quéléver, L., Schallhart, S., Dada, L., Heikkinen,
946 L., Peräkylä, O., Zou, J., Rose, C., Wang, Y., Mammarella, I., Katul, G., Vesala, T., Worsnop, D. R., Kulmala, M.,
947 Petäjä, T., Bianchi, F., and Ehn, M.: Vertical characterization of highly oxygenated molecules (HOMs) below and
948 above a boreal forest canopy, Atmos. Chem. Phys., 18, 17437-17450, 10.5194/acp-18-17437-2018, 2018.

949

950 Zhang, H., Li, H., Zhang, Q., Zhang, Y., Zhang, W., Wang, X., Bi, F., Chai, F., Gao, J., Meng, L., Yang, T., Chen,
951 Y., Cheng, Q., and Xia, F.: Atmospheric Volatile Organic Compounds in a Typical Urban Area of Beijing: Pollution
952 Characterization, Health Risk Assessment and Source Apportionment, Atmosphere, 8, 10.3390/atmos8030061,
953 2017.
954
955 Zhang, H., Zhang, Y., Huang, Z., Acton, W. J. F., Wang, Z., Nemitz, E., Langford, B., Mullinger, N., Davison, B.,
956 Shi, Z., Liu, D., Song, W., Yang, W., Zeng, J., Wu, Z., Fu, P., Zhang, Q., and Wang, X.: Vertical profiles of biogenic
957 volatile organic compounds as observed online at a tower in Beijing, Journal of Environmental Sciences, 95, 33-42,
958 https://doi.org/10.1016/j.jes.2020.03.032, 2020.
959
960 Zhang, Q., Jimenez, J. L., Canagaratna, M. R., Allan, J. D., Coe, H., Ulbrich, I., Alfarra, M. R., Takami, A.,
961 Middlebrook, A. M., Sun, Y. L., Dzepina, K., Dunlea, E., Docherty, K., DeCarlo, P. F., Salcedo, D., Onasch, T.,
962 Jayne, J. T., Miyoshi, T., Shimono, A., Hatakeyama, S., Takegawa, N., Kondo, Y., Schneider, J., Drewnick, F.,
963 Borrmann, S., Weimer, S., Demerjian, K., Williams, P., Bower, K., Bahreini, R., Cottrell, L., Griffin, R. J.,
964 Rautiainen, J., Sun, J. Y., Zhang, Y. M., and Worsnop, D. R.: Ubiquity and dominance of oxygenated species in
965 organic aerosols in anthropogenically-influenced Northern Hemisphere midlatitudes, Geophysical Research Letters,
966 34, https://doi.org/10.1029/2007GL029979, 2007.
967
968 Zhang, Y., Peräkylä, O., Yan, C., Heikkinen, L., Äijälä, M., Daellenbach, K. R., Zha, Q., Riva, M., Garmash, O.,
969 Junninen, H., Paatero, P., Worsnop, D., and Ehn, M.: A novel approach for simple statistical analysis of high-
970 resolution mass spectra, Atmos. Meas. Tech., 12, 3761-3776, 10.5194/amt-12-3761-2019, 2019.
971
972 Zhao, Y., Thornton, J. A., and Pye, H. O. T.: Quantitative constraints on autoxidation and dimer formation from
973 direct probing of monoterpene-derived peroxy radical chemistry, Proceedings of the National Academy of Sciences,
974 115, 12142, 10.1073/pnas.1812147115, 2018.
975